

Relative Localization using Satellite positioning

KARL LUNDIN

Master in Systems, Robotics and Control

Date: December 17, 2019

Supervisor: Håkan Carlsson, Linnea Persson

Examiner: Joakim Jaldén

School of Electrical Engineering and Computer Science

Swedish title: Global och relativ GNSS-positionering

Abstract

In this paper, the basis for Global Navigation Satellite Systems (GNSS) is presented and a comparison between the expected precision of the relative position between two receivers is presented based on observations made by two stationary receivers. The positioning is compared between the solution from two algorithms. The first relative estimate is based on making individual position estimates for the receivers and calculating the difference. The second uses a so called double difference method for estimating the relative position. The assumption is that systematic noises will be more successfully mitigated by the use of a double difference algorithm, which is also verified through simulations. The result of the observations is that the double difference performs slightly better, with a measured mean error of 4.8 and 4.9 m, compared to the relative position of the global estimates of 5.6 and 5 meters. These errors indicates that the random and unmodeled noises were larger in the sampling series than what was expected. A continued work should implement a filter that can lower the noise levels in the observations.

Sammanfattning

I detta dokument presenteras grunderna för Satellitnavigation (GNSS) och en jämförelse mellan den förväntade precisionen hos den relativa positionen mellan två GNSS-mottagare baserat på mätningar från två stationära mottagare. Positioneringen jämförs för lösning som erhålls som differensen mellan individuella globala positioner samt när en differentierad positionslösning implementeras. Antagandet till grund för undersökningarna är att den differentierade estimatorn är bättre på att minska effekterna av systematiska brus. Detta verifieras även med hjälp av simulerings. Den positionslösning som erhålls visar att positionen baserat uteslutande på Satellitnavigation kan förväntas ligga på strax över 5 m, med uppmätta medelfel på 5 och 5,6 m, samt strax under 5 m för den dubbeldifferentierade estimatorn med uppmätta medelfel på 4,8 samt 4,9 m. Magnituden på felet indikerar att de omodellerade brusnivåerna var större än väntat. Ett fortsatt arbete bör söka att utveckla lösningen och implementera ett filter som kan minska brusnivåerna.

I would like to express my deepest gratitude to my supervisors Håkan Carlsson and Linnea Persson who I believe have gone well beyond their expected effort and invested a lot of time in aiding me in discussing the theory and investigating the implementation. I would also like to express a thank you to family and friends who have supported me through this project.

Contents

1	Introduction	1
1.1	An introduction to Global navigation satellite systems	1
1.2	Satellite orbits	1
1.3	The idea of satellite navigation	2
1.4	Applications of GNSS-positioning	2
1.5	Other satellite navigation techniques	4
1.6	Previous research	5
1.7	Problem description and results	6
1.8	Objective	7
1.9	Scientific question	7
1.10	Delimitation	7
2	Background	8
2.1	Navigation frames and Earth representation	8
2.1.1	Coordinate frame transformation	9
2.2	The pseudorange signal and error terms	10
2.2.1	Components of the pseudorange	11
2.2.2	Pseudorange error terms	12
2.3	Satellite positioning using ephemeris data	13
2.4	Global positioning model and estimates	14
2.4.1	Global positioning observation model	17

2.5	Global positioning estimator model	18
2.5.1	Weighted estimator	19
2.5.2	Iterative steps of estimator	20
2.6	Global position estimator pseudo-code	21
2.7	Relative positioning	21
2.7.1	Differential technique observation model	23
2.7.2	Single difference estimator	23
2.7.3	Double difference estimator	24
2.8	Satellite Geometry	26
3	Method	29
3.1	Simulation of data	29
3.1.1	Testing different error sources impact on global position	29
3.1.2	RMSE of relative position from global position and DD estimate	30
3.2	GNSS positioning from observation data	31
3.2.1	Data extraction from sensor	31
3.2.2	Experimental setup	32
3.2.3	Global and relative positions from onboard estimate .	32
3.2.4	Global and relative position estimates from raw data .	33
3.2.5	Double difference relative positioning	33
4	Results	35
4.1	Error and convergence from simulated data	35
4.1.1	Convergence of estimate for noise free measurements with different initial error	35
4.1.2	Final estimate for added measurement noise of different magnitudes	38
4.1.3	Comparison of RMSE of relative position from simulated data	41

4.2	Individual and relative position estimate using global positioning	41
4.2.1	Position from onboard estimate	41
4.2.2	Global and relative position estimates from global position estimator	42
4.3	Histograms of DD-relative position estimates	47
4.4	RMSE of relative position from observation data	49
4.5	DOP values	49
4.5.1	Global position estimator DOP values	50
4.5.2	Double difference estimator DOP values	50
5	Conclusions and further work	57
5.1	Results of simulations	57
5.2	Precision of the estimates	57
5.3	DOP values	58
5.4	Further work	58
A		59
A.1	Least squares	59
A.1.1	Weighted Least Squares	60
A.2	Data structs and log format	60
A.3	Global position and onboard estimates	61

Chapter 1

Introduction

1.1 An introduction to Global navigation satellite systems

The human presence in space began with the launch of the Soviet Union's Sputnik, closely followed by the USA's Explorer satellites in 1957 and 1958 respectively. Since then, many more launches of human-made objects into space have been performed, by several different countries. For the purpose of positioning there exist several systems in parallel, among them the US "Global Positioning System" (GPS), the Russian "Globalnaja Navigatsionnaja Sputnikovaja Sistema"[Latin transliteration] (GLONASS) and the Chinese 北斗 (Eng: Beidou) are arguably the most well known. The general name for satellite systems used for navigation purposes is the "Global Navigation Satellite System" (GNSS).

1.2 Satellite orbits

Some satellites used for e.g. radio and television are in an orbit around the earth at the same angular velocity as the planet's rotation, known as a geostationary orbit which implies that the satellite will stay over the same point on the surface of the earth. These satellites will travel along an orbit with a radius of 42.000 km or at a distance of around 36.000 km above the Earth's surface [1].

The GNSS satellites travel at a shorter distance and thus have a shorter orbital period. For the GPS system, the average distance is 20.200 km which gives them a base orbit period of around $\frac{1}{2}$ day. The other GNSS systems behave similarly to this. The distance to Earth is not constant over time since the satellite orbits will in practice always have some level of eccentricity, meaning that their path is elliptic with a center that may be far from the Earth's center. For navigation satellites, this eccentricity is generally small, below 0.02 meaning that the orbit is close to a circle [2].

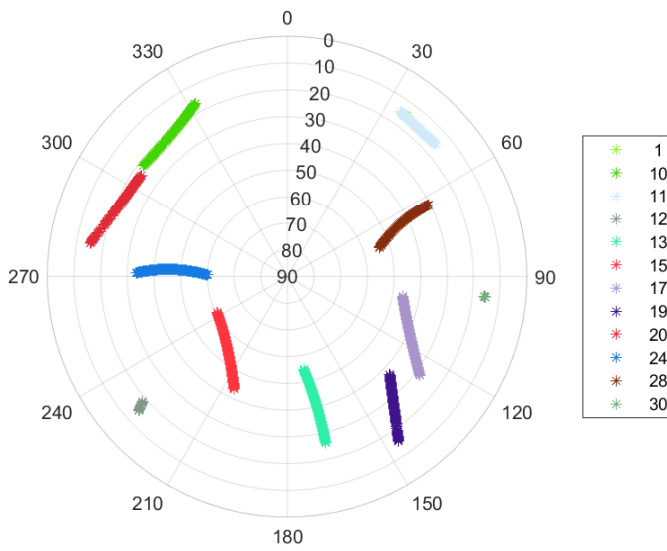
The skyplot of GPS-satellites, in relation to the receiver's position from real observations is shown in figure 1.1. The plots are shown for satellite positions over the horizon and degrees clockwise from the north direction. The method for calculating the satellite position will be presented in section 2.3.

1.3 The idea of satellite navigation

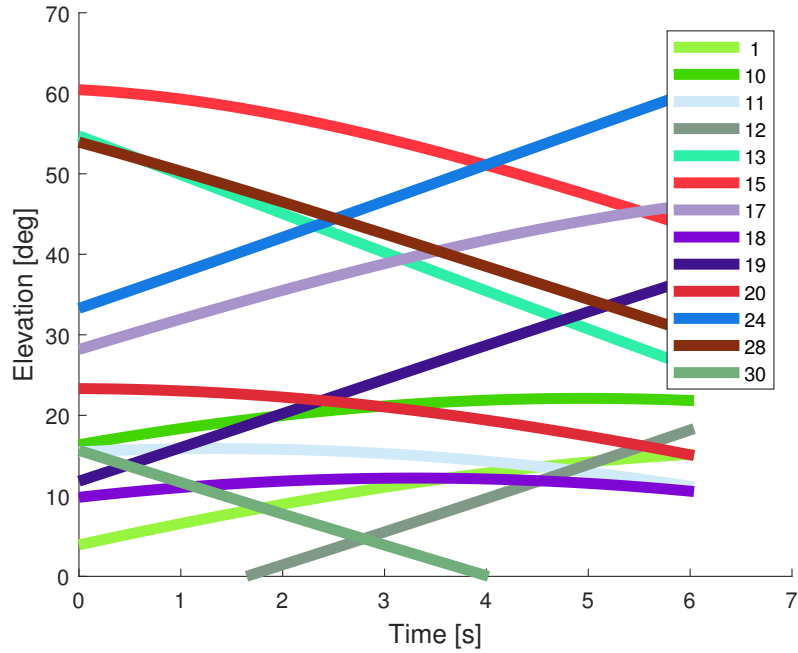
The process of determining a GNSS-receiver's position on earth is based on comparing its distance to a number of satellites whose position is known by the receiver in a process called trilateration. The idea is illustrated in an ideal and noise free 2-dimensional case in figure 1.2 for two, three and four senders. The circles represent the radial distance to a satellite. For 2 senders, the solution is generally underdefined as multiple positions are valid. In a planar case that is illustrated with the two dots. In a 3D case, the solution space would form a circle at the intersections of the radius spheres. A unique solution only exists if both observations are equal to the corresponding radii and the circle collapses to a point. For three senders a unique solution is available and for four or more the system is overdetermined.

1.4 Applications of GNSS-positioning

The use of GNSS-positioning has spread from its original military purpose to being an integrated part of many applications, both business and consumer-oriented. The usage of positioning through satellite navigation is today widely spread and has numerous applications, such as being present in many modern cellphones, ships and cars. The advantages include its global usability for outdoor conditions as well as providing accuracy mostly within 5 meters at any time of the day [3].



(a) Elevation in degrees over the horizon on radial axis and degrees clockwise from north direction on the angular axis.



(b) Elevation in degrees over the horizon over time.

Figure 1.1: Skyplot of GPS-satellites in the sky over the receiver, recorded on April 11th 2019, for one hour from 08:46 UTC. In (a), satellites are only plotted for when they are observed. Observations made in Stockholm, Sweden.

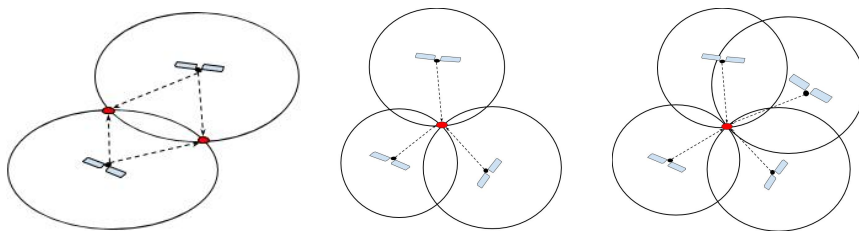


Figure 1.2: Example of positioning based on radial distance between sender and receiver for 2 (left), 3 (middle) and 4 (right) senders. The circles represent the distance from the sender and should be spherical, but is illustrated in 2D.

In some applications, only the relative position between two units is of importance, e.g. for a ship docking or when landing on a platform. In this context the absolute position may be irrelevant and an offset from the true position does not influence the process, provided that both estimates contain the same offset. The simplest method of getting a relative position given two global positions is to calculate the difference between the positions. If a very high precision of the relative estimate is required, meaning that the error in the relative position estimate must be very low, this method may be insufficient as any error in the estimate of individual global positions may sum to a larger error. Then the use of some other technique which is better able to reduce the effect of the noise into the estimate may be superior to the trivial relative method. Different techniques have been developed to achieve a significantly higher precision than that available from standalone positioning. A few of these techniques will be presented in section 1.5.

In the future, the use of satellite positioning may become an even more integrated part of our society as the potential to obtain a position estimate correct to within a few centimetres may lead to revolutions in many industries. Two examples are farming, when tractors may work the field unsupervised virtually without overlap in its path [4] or the potential for autonomous delivery of medical or customer goods using drones [5].

1.5 Other satellite navigation techniques

Three techniques which build on the idea presented in section 1.3 worth describing briefly are the differential technique, Differential GPS (DGPS) and Real Time Kinematic (RTK).

Differential techniques are based on using the direction to a transmitter rather

than its position to estimate a relative distance between two points. The methods use that the scalar product between the direction vector and the relative distance is equal to the difference in distance to the transmitter. This way a relative position between two receivers can be calculated. Differential methods can be implemented as single, double or triple difference, where the use of double difference (DD) will be important in this paper.

DGPS is a form of differential technique where a base station with a known position is used for reference. The base station can then transmit correction factors for the satellite signals to the other receiver, called a rover.

The RTK method is a further development of the differential techniques, which utilizes the difference in phase between the signal for a base station and the mobile receiver. Commonly the L1 and L2 band of respectively 1575.42 MHz and 1227.60 MHz are used, which results in a wavelength of around 20 cm. The number of cycles between the receivers needs to be calculated. If the number of cycles is correct, the position can be calculated at a very high accuracy from the difference in phase.

1.6 Previous research

GNSS systems have been available for decades and much research has been performed on the behavior of the systems. Specifically, on the topic of the DD technique, research presented in [6] shows an implementation of a weighted least squares solution based on the signal strength for a pair of stationary receivers on a rooftop. The error of the estimate is presented in relation to the true baseline, where for two different baselines of 3 m and 8 m respectively, an error of respectively 3.2 m and 3.6 m is presented.

In [7], research on similar techniques as in [6] is presented. One addition is that the estimates are performed in different environments with a 3 m baseline. For an open space environment, a mean error of 0.6-0.7 meter is achieved, for an environment with surrounding trees the measures mean error was 4 m and in the vicinity of buildings 2.3 m which indicate that noise levels in the observations may be very dependant on the environment. As stated in the article: "This indicates that obstacles such as buildings and trees cause higher noise of GPS measurements".

In [8], the DD-technique is presented which achieves an error in position fix of less than 1 m error for the receiver positions is. This is an example based on

an experimental setup where any noise stemming from signal reflection can be expected to be zero as the receivers share the antenna between them and is unlikely to be achieved for real applications.

In [9], the performance of DGPS is evaluated as a function of the distance to the base station. The results from measurements from stationary DGPS receivers at a known distance show that the position with 95% probability is correct to within 0.5-1 m near the base station and grows with 0.2 m per 100 km separation.

In [10] an RTK-solution is implemented and tested for baselines of 2-31 km, showing an accuracy of respectively 1 cm and 2 cm horizontally and vertically.

1.7 Problem description and results

This report presents the work that has been done with computing a relative position for the GNSS-INS receiver provided by inertial sense. It is a multi-sensor unit where either measurements from a single sensor, or the fused information from several, can be extracted. The data from "MEMs gyros, accelerometers, magnetometers, barometric pressure, and GPS/GNSS is fused to provide optimal estimation"¹. Data has been logged by sampling from stationary sensors and processed using MATLAB.

The results are based on the raw GNSS observation data sampled from the units and are presented in two ways: The relative position from the units from

- (i) A difference between individual position estimates.
- (ii) A Double Difference method.

The results show that for (i), the mean error can be expected to be in the magnitude of slightly above 5 m, with measurement mean values of 5 and 5.6 m. For (ii) the position error can be expected to be slightly below 5 m, with measurement mean values of 4.9 and 4.8 m. For future work a few improvements are suggested: data from other sensors may be fused to produce an even finer solution as well as the solution being produced in real-time. In addition to that, implementing a filter should be able to reduce much of the high frequency noise in the observations and lower the mean error.

¹<https://inertialsense.com/%C2%B5ins-dual/> (2019-12-11)

1.8 Objective

The objective of this report is to investigate the relative positioning estimate based on two different methods and compare them. The two algorithms which are implemented are based on difference between the positions in the individual position estimates and the DD-based relative position. The results are presented for standard deviation in position per direction and the calculated mean error.

1.9 Scientific question

The purpose of this paper is to investigate what precision in the positioning that can be expected from a GNSS-solution for the purpose of the automated landing process. This is reflected in the question, formulated below.

- What precision can be expected from a relative GNSS-solution between two receivers using difference in global position fix and differentiated methods.

Ideally an estimate that is correct to within half a meter would ensure that the landing can be made safely.

1.10 Delimitation

Many applications, such as those mentioned above, are implemented as solutions to mobile problems. This investigation is limited to sampling from two receivers under stationary conditions, using a known distance. The results are also only presented for solutions presented from logged data. No real-time solution is implemented.

Chapter 2

Background

This section explains the theory behind:

- Important coordinate frames for representation and their relationship.
- How observations are made, modelled and the observation error sources.
- How satellite positions are calculated.
- How a global position estimate and differenced relative estimates are calculated.
- How satellite geometry influences the estimate.

2.1 Navigation frames and Earth representation

In order to navigate in a 3D-world, a set of three vectors need to be defined. There exist global frames, which may be used for positioning anywhere, as well as local frames which are defined with directions and origin at an arbitrary point. There are several coordinate frames for a point in a GNSS application, among those the notable ones are the Longitude-Latitude-Altitude (LLA), Earth-Centered-Earth-Fixed (ECEF) and North-East-Down representations (NED). All systems presented follow the rotation of the earth. It is also implied that the standard is based on the WGS84 system as it is the basis for GPS.

LLA: The LLA-system is a spherical system, using the angular arguments degrees West of the Greenwich meridian, denoted λ and North of the equator, denoted ϕ , as well as a straight coordinate height over the surface of the earth. The altitude argument relies on a reference to the model of the earth that is used, where 0 altitude implies being on the surface.

ECEF: The ECEF system is a Cartesian system, where the x and y-axes go through the equator with the x-axis pointing through the 0-meridian and the z-axis straight north.

NED: A NED-coordinate system is defined locally at an arbitrary point such that the axes point respectively straight in the north, east and down direction, where down implies towards the center of the earth.

Elevation Azimuth: The Elevation-Azimuth system is a spherical system defined locally. The radius can also be introduced to turn it into a 3D system. Elevation implies the degrees above the horizon and Azimuth the degrees clockwise from the north direction. This works well for an origin at a low altitude as the zero degrees defined by the horizon will be perpendicular to the radial direction of the earth, but for a higher altitude the angle to the horizon will become negative and this frame may lose its utility.

2.1.1 Coordinate frame transformation

The different coordinate systems representations are illustrated in figure 2.1. The transformation between a point B in an ECEF frame to a local NED-frame around a point A is given as a combination of two rotation matrices. First a rotation around the longitude $R_1(\lambda)$, followed by a rotation of the latitude $R_2(\phi)$. These rotation matrices are given by:

$$R_1(\lambda) = \begin{bmatrix} -\sin \lambda & 0 & \cos \lambda \\ 0 & 1 & 0 \\ -\cos \lambda & 0 & -\sin \lambda \end{bmatrix} \quad (2.1)$$

and

$$R_2(\phi) = \begin{bmatrix} \cos \phi & \sin \phi & 0 \\ -\sin \phi & \cos \phi & 0 \\ 0 & 0 & 1 \end{bmatrix} \quad (2.2)$$

and finally the rotation matrix $R = R_1 \cdot R_2$ gives the coordinate transformation

$$\begin{bmatrix} n \\ e \\ d \end{bmatrix} = \begin{bmatrix} -\sin \lambda \cos \phi & -\sin \lambda \sin \phi & \cos \lambda \\ -\sin \phi & \cos \phi & 0 \\ \cos \lambda \cos \phi & -\cos \lambda \sin \phi & \sin \lambda \end{bmatrix} \begin{bmatrix} \Delta x \\ \Delta y \\ \Delta z \end{bmatrix} \quad (2.3)$$

where n, e, d represents the position in the local frame, λ and ϕ the longitude and latitude angles of the point of transformation and $\Delta x, \Delta y, \Delta z$ the difference between points A and B in ECEF-coordinates. The rotation matrix R_2 also coincides with the rotation of the earth. A property of a rotation matrix M is that for any rotation ζ around a single axis, the inverse rotation is equivalent to its transpose, such that $M(-\zeta) = [M(\zeta)]^T$.

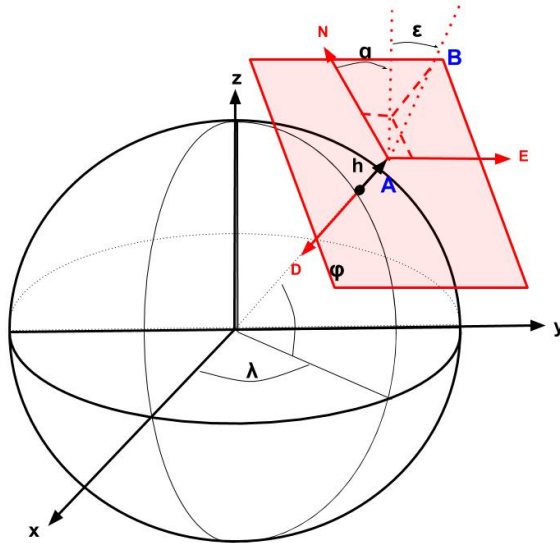


Figure 2.1: Commonly used coordinate frames for GNSS navigation and their correlation is shown. Global frames: ECEF, defined by directions x,y,z. LLA, defined by angles λ, ϕ and height h . Local frames around a point \mathbf{A} where the plane in red is tangential to the surface: NED, defined by the directions $\mathbf{N}, \mathbf{E}, \mathbf{D}$, and Elevation Azimuth for a point \mathbf{B} with regards to point \mathbf{A} given by α degrees clockwise from north and ϵ degrees above the horizon.

2.2 The pseudorange signal and error terms

The primary source of data for GNSS positioning is called the pseudorange and is based on calculating a time difference between transmission and reception which can be translated to a range through the speed of light. The specific method for measurement acquisition is based on sampling a sequence of the pseudorandom code sent out by a satellite, which is then compared for similarity to a longer sequence by the receiver. This gives the receiver information

about when the signal was broadcast, while the time of reception is based on the receiver clock. Since in this project, the pseudorange will be sampled directly in the form of a distance from the receiver, the discussion on observation acquisition will not be explained further, more information on the specifics of how the signal is sampled can be found in [2].

2.2.1 Components of the pseudorange

The pseudorange signal is measured as a time difference between time of transmission and reception. Both clock times are assumed imperfect and containing an offset from the true time, which will impact the measurement. The measurement is considered a sum of three parts: the time difference between the true times of transmission and reception, the time difference between the respective clock offsets, and an error term [11]. The model for these clock offsets are discussed further in section 2.2.2.1. The measured time of propagation, T_{prop} is then expressed as

$$T_{prop} = (t_{rec} - t_{tr}) + (\Delta t_{rec} - \Delta t_{sat}) + \nu. \quad (2.4)$$

where t_{rec} and t_{tr} are the true times of reception and transmission, Δt_{sat} and Δt_{rec} the transmitter and receivers respective offset from the true time in seconds and ν and error term, discussed further in section 2.2.2.2. The propagation time for the signal is, with previously mentioned orbit, at around 6-7 ms and is the sought after component of the signal since it tells the distance to the sender. The measurement is transformed to a distance by multiplying with the speed of light c , and an observation can instead be expressed as a function of the actual distance and clock difference as

$$y = \|\mathbf{p}^{sat} - \mathbf{p}_{rec}\| + c\Delta t + c\nu \quad (2.5)$$

where \mathbf{p}^{sat} and \mathbf{p}_{rec} are the positions of the sender and receiver respectively. The use of bold font, e.g. \mathbf{p} will be used forwards to indicate a vector.

The function h defined as

$$\begin{aligned} h(\mathbf{p}^{sat}, \mathbf{p}_{rec}, \Delta t_{rec}) &= \|\mathbf{p}^{sat} - \mathbf{p}_{rec}\| + c\Delta t_{rec} \\ &= \sqrt{((p_x^{sat} - p_x)^2 + (p_y^{sat} - p_y)^2 + (p_z^{sat} - p_z)^2)} + c\Delta t_{rec}. \end{aligned} \quad (2.6)$$

is introduced, turning equation (2.5) into

$$y = h(\mathbf{p}^{sat}, \mathbf{p}_{rec}, \Delta t_{rec}) - c\Delta t_{sat} + c\nu \quad (2.7)$$

$$= h(\mathbf{p}^{sat}, \theta) - c\Delta t_{sat} + c\nu. \quad (2.8)$$

The argument $\theta = [\mathbf{p}_{rec}, \Delta t_{rec}]$ has been introduced to represent the receiver state vector. The arguments of h are the primary variables to estimate, but before the method to obtain an estimate can be explained, more underlying theory must be presented.

2.2.2 Pseudorange error terms

The different components of the error term ν , mentioned in section 2.2.1 are explained and given an expected range in this section. A summary of the noise sources can be found in table 2.1.

2.2.2.1 Clock errors

The clocks in satellites are very precise, but as many of them have been active for a long time, the error can still amount to large values due to error build up over a long time. This error is called a bias and originates in the clock time advancing slightly different from an ideal clock, called a drift. This drift can be modeled as a random walk behavior and means that the error tends to build up slowly over time. The bias in receivers can often be much larger with a much higher drift. However between two consecutive samples, the difference is small, e.g: an average drift of +1 second/day translates to $\sim 10\mu s/s$. The clock biases give rise to a positioning error in two parts where the first part is the range error included in eq. (2.5). These biases should be taken into account since a clock error of 1 ms can result in a positioning error of thousands of kilometers as $1\text{ ms of clock bias equals to } c \cdot 0.001s \approx 3 \cdot 10^5\text{ m}$.

The second part of the clock bias positioning error stems from that the satellite position is determined with time as an argument, parametrized by a set of equations from the ephemeris data, explained more below. The receiver bias constitutes the largest part as an error in the receiver clock will lead to an error in the satellite position. The GNSS satellites travel at a speed of around 4000 m/s which means that a receiver clock error of $\Delta t_{rec} = 0.01\text{ s}$ can result in an error in the satellite position of around 40 m. Both the satellite and receiver clock errors will be compensated for, explained in section 2.3 and 2.5. The remaining error in the satellite clock after correction is in the range of 2.5 m [2].

2.2.2.2 Other error sources

The third part of the signal, the noise terms ν , is composed of several parts. This can be split up into a common noise and non common noise, where a common noise implies that it is equal for two simultaneous observations separate in space. If the common noise is expressed it will be denoted η . Otherwise, it will be included in the unmodelled noise sources, denoted ϵ .

The common noises include the Ionospheric and Tropospheric atmospheric noise, which can range up to 100 m [12] and 25 m [13] respectively, but mostly are in the range of about 5 m and 0.5 m respectively [2]. There are models for how to compensate for these effects, presented e.g. in [14] but they are not modeled in this project. Another common noise is the error in calculated position of the transmitting satellite, discussed further in section 2.3. The satellite position calculation is correct to in average 1 m in any direction [15].

The unmodelled noise sources include multipath effects which is when signals are reflected off other objects, as well as receiver noise. These noise sources can be expected to be in the range of 1 and 0.3 m respectively [2], but examples of multipath has been observed up to 100 m [14].

Noise Source	Range [m]
Satellite Clock	2.5
Satellite Orbit	1
Ionosphere	5
Troposphere	0.5
Multipath	1
Receiver error	0.3

Table 2.1: Noise sources in the range observations with a normal error range.

2.3 Satellite positioning using ephemeris data

In order to determine a receiver's global position using satellites, the satellite's position should be known. The satellite positions at a given time are accessible online in real-time¹ or can be calculated directly. The calculations

¹E.g. from gnssplanning.com

can be done using either almanac or ephemeris data. Almanac data is a pre-defined base orbit of lower accuracy which is updated on an approximately daily basis which is readily available online² as well as satellites transmitting it directly. Precise positioning applications will rely on ephemeris data, which contains the parameters to calculate a more precise position of the satellite. This is transmitted by the individual satellite at a frequency of a few times per minute.

The data contained in the ephemeris message is based on the set of Keplerian equations which describes an orbit in space. Each message will contain information of 20 parameters: two reference times, three clock correction factors, six Keplerian parameters and nine perturbation parameters.

The clock correction factors are specific to each satellite and are the primary form of clock correction, used to correct for the Δt_{sv} term in (2.4). The equation to calculate the satellite clock bias, the precise algorithm for calculating the position and description of the Keplerian equations can be found in [16]. An example of the parameters in an ephemeris message used for this project is shown in figure 2.2. The satellite position is then calculated using the corresponding ephemeris data with time as an argument and will be given in an ECEF frame.

It is relevant to note that the time applied in the GPS-system is zeroed at Midnight January 6, 1980, and expressed in the format number of weeks and time of the week in seconds, using midnight Sunday-Monday as reference.

2.4 Global positioning model and estimates

To estimate a position in 3D as well as the receiver clock bias a minimum of 4 transmitting satellites is needed. Utilizing the pseudorange measurements in combination with knowledge of the satellite's position at the time of transmission, a position estimate can be calculated. The receiver and satellite position are 3×1 -vectors $[x, y, z]$ conveniently expressed in an ECEF frame, as that is how satellite positions are given in calculations presented in section 2.3. To solve this with regards to the currently unknown θ , an iterative linearized solver can be implemented, presented below. For clarity, the values that are estimated and those calculated are as follows:

²E.g. from <https://www.navcen.uscg.gov/>

satID	2
iode	110
iodc	110
week	2078
toe	309600
toc	309600
ttr	304836
A	2.6559e+07
e	0.0193
i0	0.9569
OMG0	0.3503
omg	-1.7032
M0	-2.1420
deln	4.7070e-09
OMGd	-7.9675e-09
idot	4.0109e-10
crc	288.5625
crs	19.5938
cuc	1.2275e-06
cus	4.3046e-06
cic	2.7195e-07
cis	1.2293e-07
toes	309600
f0	-3.4128e-04
f1	-7.7307e-12
f2	0

Table 2.2: An example of a sample of the parameters contained in a single ephemeris message sampled on November 7, 2019.

Estimates The following are estimates in the model:

- \mathbf{p}_{rec} : Receiver position in [m] (ECEF), vector 1×3 .
- Δt_{rec} : Receiver clock bias [s], scalar value.
- \mathbf{p}^{sat} : Satellite position [m] at time of transmission (ECEF), vector 1×3 .
- τ : Time of flight [s] for GNSS-signal, scalar value.
- t : Observation time, seconds of week in GPS-time [s] that signal was received by the receiver, scalar value.
- t_{tr} : Time of transmission [s], scalar value.
- γ : Earth's rotation [rad] during signal time of flight, scalar value.

Calculated or given values These values are either given or directly calculated given values.

- y : Pseudorange observation [m], scalar value.
- Δt_{sv} : Satellite clock bias [s], scalar value.
- t_{rec} : Nominal time of reception as registered by the receiver, not considering receiver clock bias, scalar value [s].
- ξ : Ephemeris parameters, transmitted by each GNSS-satellite individually.
- ϵ : Unmodeled error source.

Any set of values or estimates will be ordered as a column vector, e.g. $\mathbf{y} = [y^1 \dots y^n]^T$ is a $n \times 1$ vector of pseudorange observations, where a superscript is used as an index to indicate corresponding satellite and observation.

Satellite position Satellite positions are calculated using the transmitted information in the ephemeris data as described in chapter 2.3. For a satellite, the position is calculated using only t as an argument, and parametrized by the ephemeris values in ξ :

$$\mathbf{p}^{sat}(t; \xi). \quad (2.9)$$

Time of flight The time of flight is the propagation time of a signal between two arbitrary points p_1 and p_2 . This will be of relevance as the satellite position has changed between times t_{tr} and t . It is calculated as

$$\tau = \frac{1}{c} \|\mathbf{p}_1 - \mathbf{p}_2\| \quad (2.10)$$

Time of transmission Time of transmission for satellite signal is then calculated as

$$t_{tr} = t - \tau. \quad (2.11)$$

Earth's rotation The angle of rotation for a point on earth during τ seconds is given by

$$\gamma = \tau \cdot \omega_e \quad (2.12)$$

Rotated satellite position Equations (2.9-2.12) allow for calculating the position of a satellite at t_{tr} as well as correcting for the rotation of the ECEF coordinate system during τ seconds. The satellite position is calculated at t_{tr} and then rotated, resulting in the position $\mathbf{p}'(t_{tr}; \gamma)$ in ECEF-coordinates is given by applying a rotation matrix to the position $\mathbf{p}^{sat}(t_{tr})$.

$$\mathbf{p}'(t_{tr}) = \begin{bmatrix} \cos(\gamma) & \sin(\gamma) & 0 \\ -\sin(\gamma) & \cos(\gamma) & 0 \\ 0 & 0 & 1 \end{bmatrix} [\mathbf{p}^{sat}(t_{tr})]^T \quad (2.13)$$

where the rotation applied is the counter clockwise rotation given by transposing (2.2).

Satellite clock bias The satellite clock bias is calculated at nominal time t_{rec} using the information in ξ and considered a constant for a single observation.

$$\Delta t_{sv}(t; \xi) \quad (2.14)$$

2.4.1 Global positioning observation model

A single observation y is modelled as

$$y = h(\mathbf{p}'(t_{tr}), \boldsymbol{\theta}) - \Delta t_{sv} + \epsilon \quad (2.15)$$

which is the same as (2.7), with the exception that the satellite position is given by \mathbf{p}'_{sat} , given by equation (2.13) and ν has been replaced by ϵ to indicate that it is not modelled. Thus the full model of an expected observation \hat{y} , given satellite position and receiver states is given by

$$\hat{y} = \|\mathbf{p}'(t_{tr}) - \mathbf{p}_{rec}(t)\| + c \cdot (\Delta t_{rec}(t) - \Delta t_{sv}) \quad (2.16)$$

where the unmodelled error ϵ is omitted.

2.5 Global positioning estimator model

The purpose of the equations presented above is to reach a solution for the receiver states \mathbf{p}_{rec} and Δt_{rec} . The actual implementation is an iterative process where estimates are updated until convergence. For the sake of presenting the governing model, any variable should be interpreted as the current estimate, which will then be updated at the next iteration until convergence is attained. For a set of n observations \mathbf{y} and the corresponding satellite positions P^{sat} which is a $3 \times n$ matrix, equation (2.7) can be expressed as:

$$\mathbf{y} = h(P^{sat}, \boldsymbol{\theta}) + \Delta t_{sv} + \boldsymbol{\epsilon} \quad (2.17)$$

$$= \begin{bmatrix} h^1(\mathbf{p}^{(1)}, \boldsymbol{\theta}) \\ \vdots \\ h^n(\mathbf{p}^{(n)}, \boldsymbol{\theta}) \end{bmatrix} + \begin{bmatrix} \Delta t_{sv}^1 \\ \vdots \\ \Delta t_{sv}^n \end{bmatrix} + \begin{bmatrix} \epsilon_1 \\ \vdots \\ \epsilon_n \end{bmatrix} \quad (2.18)$$

The satellite clock errors Δt_{sv} will be subtracted from (2.18) using the equation in [16] to get

$$\mathbf{y}^* = h(\mathbf{p}^{sat}, \boldsymbol{\theta}) + \boldsymbol{\epsilon} \quad (2.19)$$

$$= \begin{bmatrix} h^1(\mathbf{p}^{(1)}, \boldsymbol{\theta}) \\ \vdots \\ h^n(\mathbf{p}^{(n)}, \boldsymbol{\theta}) \end{bmatrix} + \begin{bmatrix} \epsilon_1 \\ \vdots \\ \epsilon_n \end{bmatrix} \quad (2.20)$$

These equations are solved for the estimate $\hat{\boldsymbol{\theta}}$ such that the error

$$\|\mathbf{y}^* - h(P^{sat}, \boldsymbol{\theta})\|^2 \quad (2.21)$$

between observations and expected observations are minimized

$$\hat{\boldsymbol{\theta}} = \underset{\boldsymbol{\theta}}{\operatorname{argmin}} \left(\|\mathbf{y}^* - h(P^{sat}, \boldsymbol{\theta})\|^2 \right). \quad (2.22)$$

The system of equations is solved using the gradient of the equations. The gradient of the observation model equation (2.16) is for a satellite i

$$\begin{aligned}\frac{\partial}{\partial \boldsymbol{\theta}} h^{(i)}(\mathbf{p}^{(i)}, \boldsymbol{\theta}) &= \frac{\partial h(\mathbf{p}^{(i)}, \boldsymbol{\theta})}{\partial x} + \frac{\partial h(\mathbf{p}^{(i)}, \boldsymbol{\theta})}{\partial y} + \frac{\partial h(\mathbf{p}^{(i)}, \boldsymbol{\theta})}{\partial z} + \frac{\partial h(\mathbf{p}^{(i)}, \boldsymbol{\theta})}{\partial \Delta t} \\ &= -\frac{p_x^{(i)} - p_x}{\|\mathbf{p}^{(i)} - \mathbf{p}\|} - \frac{p_y^{(i)} - p_y}{\|\mathbf{p}^{(i)} - \mathbf{p}\|} - \frac{p_z^{(i)} - p_z}{\|\mathbf{p}^{(i)} - \mathbf{p}\|} + c \\ &:= \nabla h^{(i)}(\mathbf{p}^{(i)}, \boldsymbol{\theta})\end{aligned}\quad (2.23)$$

All the gradients in (2.23) are collected in a $n \times 4$ matrix \mathbf{H} :

$$H(P^{sat}, \boldsymbol{\theta}) = \begin{bmatrix} \nabla h^1(\mathbf{p}^1; \boldsymbol{\theta}) \\ \vdots \\ \nabla h^n(\mathbf{p}^n; \boldsymbol{\theta}) \end{bmatrix}. \quad (2.24)$$

The result of (2.24) leads to the least square solution of (2.22) being expressed as:

$$\hat{\boldsymbol{\theta}} = (H^T \cdot H)^{-1} H^T \mathbf{y}^*, \quad (2.25)$$

as described in A.1. Equation 2.25 is a step in a Gauss-Newton iterative process where a step is expressed as

$$\begin{aligned}\boldsymbol{\theta}^{(j+1)} &= \boldsymbol{\theta}^{(j)} - \hat{\boldsymbol{\theta}} \\ &= \boldsymbol{\theta}^{(j)} - (H^T(\boldsymbol{\theta}^{(j)}) H(\boldsymbol{\theta}^{(j)})^{-1} H^T(\boldsymbol{\theta}^{(j)})(\mathbf{y} - h[P^{sat,(j)}, \boldsymbol{\theta}^{(j)}])\end{aligned}$$

where the superscript (j) indicates an iteration number.

2.5.1 Weighted estimator

If there is knowledge of the uncertainty in the observations, the minimizing function in 2.22 can be described by

$$\hat{\boldsymbol{\theta}} = \operatorname{argmin}_{\boldsymbol{\theta}} (||\mathbf{y} - h(P^{sat}, \boldsymbol{\theta})||_W^2). \quad (2.26)$$

where $||X||_W^2 = X^T W X$ and W is a matrix of weights. The observations are not considered equal, instead observations which are more accurate are assigned a higher weight which leads to a larger impact on the estimate. In [17], the signal-to-noise-ratio (SNR), which is closely related to the CNR and

is recorded by the receivers is used as an estimate of the magnitude of the noise. It is assumed that the observations are uncorrelated, which means that the weight matrix can be described as a diagonal matrix $W = \text{diag}(w_1, \dots, w_n)$ for n observations. A weight w_i , corresponding to observation $y^{(i)}$ and its corresponding registered SNR⁽ⁱ⁾ value in dBHz are calculated as

$$w_i = 10^{-0.1 \cdot \text{SNR}^{(i)}}. \quad (2.27)$$

Equation (2.25) will then be expressed using a so called Best Linear Unbiased Estimator (BLUE), given by

$$\hat{\boldsymbol{\theta}}_{\text{BLUE}} = (H^T W H)^{-1} H^T W \mathbf{y}, \quad (2.28)$$

As described in A.1.1.

2.5.2 Iterative steps of estimator

An epoch will be used to describe a set of observations made at the same instance and will be denoted by $[k]$. The final estimate, meaning the last iteration of the state estimates, will be denoted $\boldsymbol{\theta}[k]$. For the first epoch, $k = 1$ The initial estimate of the receiver states $\boldsymbol{\theta}_0[1]$ is set to zero, i.e. $\mathbf{p}_{\text{rec}}^{(0)}[1] = [0, 0, 0]$ and $\Delta t_{\text{rec}}^{(0)}[1] = 0$. For the subsequent epochs, $k > 1$, the final estimate of the previous epoch is used as initial estimate, i.e. $\boldsymbol{\theta}_0[k + 1] = \boldsymbol{\theta}[k]$. The calculations to obtain (2.22) are in the order:

0. Calculate all $\Delta \mathbf{t}_{sv}$ for the satellites at time of reception t and adjust the observations $\mathbf{y}^* = \mathbf{y} - \Delta \mathbf{t}_{sv}$. This step is not repeated.
1. Adjust the observation for the receiver clock bias $\mathbf{y}^{**} = \mathbf{y}^* - c \Delta \mathbf{t}_{\text{rec}}$.

For each satellite individually:

2. Calculate signal time of flight $\tau^{(i)} = \frac{(\mathbf{y}^{(i)})^{**}}{c}$.
3. Calculate the satellite positions $\mathbf{p}^{(i)}(t_{\text{rec}} - \tau^{(i)}; \xi)$.
4. Calculate the rotation angle $\gamma^{(i)}$.
5. Adjust the satellite position as in (2.13) to obtain $(\mathbf{p}^{(i)})'(t_{\text{tr}})$.

6. Calculate $\hat{\theta}$ from $\mathbf{p}'(t_{tr})$, \mathbf{y}^{**} and θ as in equation (2.25) or (2.28).

This is continued until convergence in the position estimate for steps 2-7, where the convergence threshold has been set to 10^{-3} m, indicating that

- The variables \mathbf{y}^{**} , τ , \mathbf{p}_{rec} and Δt_{rec} all are interdependent.
- \mathbf{p}^{sat} , is dependant only on Δt_{rec} and τ .
- γ is dependant only on τ .
- t is dependant only on t_{rec} and Δt_{rec} .

2.6 Global position estimator pseudo-code

For the first epoch, the initial values of the receiver $\theta_0[1]$ are set to 0. For any succeeding epoch $k > 1$, the initial estimate of the states $\theta_0[k]$ will use the final estimate of the previous epoch $\theta[k - 1]$.

To calculate the receiver states during one epoch, all the estimated values are dependent on each other and any calculation will use the values calculated in the previous iteration of the others as input. In the code, the last iteration is denoted with a hat symbol, e.g. $\hat{\mathbf{p}}_{rec}$ and superscript is indexed by (i).

The function "estimate_satellite_clock_bias" is that from equation (2.14). "get_satellite_position" comes from equation (2.9). The rotation matrix in (2.13) is represented by R and the "estimate_position" function is the least squares solution to (2.25).

In the pseudo-code in algorithm 1, the set of satellite positions P_{sat} is a $n \times 3$ matrix, for a set of n satellites where an index j relates to the corresponding satellite position $\mathbf{p}^{(j)}$. It is assumed that the set $\Xi = \{\xi^{(1)}, \dots, \xi^{(n)}\}$ contains only the ephemeris data of the active satellites in each epoch. As it is a linearised system, the values of $\mathbf{y}, \tau, \mathbf{p}^{sat}, \gamma, \mathbf{p}_{rec}$ and Δt_{rec} will be updated per each iteration.

2.7 Relative positioning

Relative positions can be calculated through the difference in positions calculated as in section 2.5.2. In this section a relative estimate using a DD-method

Algorithm 1 Global position estimator pseudocode

1. Calculate satellite clock bias at observation time for each satellite
for all j in Ξ **do**
 $\Delta t_{sv}(j) \leftarrow \text{estimate_satellite_clock_bias}(t, \Xi(j))$
end for

2. Adjust the observations for Δt_{sv}
for all j in Ξ **do**
 $y(j) \leftarrow y(j) - c\Delta t_{sv}(j)$
end for
 $\Delta p \leftarrow 100$
 $\Delta b \leftarrow 100$

3. Iterate until convergence: calculate receiver states
while ($|\Delta p|$ or $|\Delta b| > 0.1$) **do**

3.1 Calculate signal time of flight
for all j in y **do**
 $y(j) \leftarrow y(j) - c\Delta t_{rec}$
 $\tau(j) \leftarrow y(j)/c$
end for

3.2. Calculate the satellite position, rotation and rotated position
for all j in Ξ **do**
 $P_{sat}(j) \leftarrow \text{get_satellite_position}(\Xi(j), t - \tau(j))$
 $\gamma(j) \leftarrow \omega_e \cdot \tau(j)$
 $P_{sat}(j) \leftarrow R(\gamma(j)) \cdot P_{sat}(j)$
end for

3.3 Estimate p_{rec} and Δt_{rec}
 $\hat{p}, \hat{\Delta t}_{rec} \leftarrow \text{estimate_position}(P_{sat}, y, p_{rec}, \Delta t_{rec})$
 $dp \leftarrow p_{rec} - \hat{p}$
 $db \leftarrow \Delta t_{rec} - \hat{\Delta t}_{rec}$
 $p_{rec} \leftarrow \hat{p}$
 $\Delta t_{rec} \leftarrow \hat{\Delta t}_{rec}$

end while

is presented. The idea is to create an estimate of the relative distance between two positions by using the shared information between two receivers. It is based on the fact that for two unit vectors $\mathbf{u}_a^{(i)}$ and $\mathbf{u}_b^{(i)}$ both pointing from receivers a and b respectively at position \mathbf{p}_a and \mathbf{p}_b , to the same satellite at position $\mathbf{p}^{(i)}$ are considered to be parallel, as the angle α between $\mathbf{u}_a^{(i)}$ and $\mathbf{u}_b^{(i)}$ is very small. The idea is presented in figure 2.2. This is motivated by that the satellite distance is generally much larger than the distance between any two points on earth. For example, an isosceles triangle, a triangle where two sides are of equal length, where the two receivers are at a distance of 1 km and the satellite at a distance of $2 \cdot 10^7$ m result in α being smaller than 0.05° . The threshold for two observations considered close is set to 10 ms. If the observations are separated by more than that the entire epoch is discarded.

2.7.1 Differential technique observation model

For the differential techniques presented below, the equation for a pseudorange measurement for the two receivers and a shared satellite i , at a given epoch will be:

$$y_a^i = \rho_a^{(i)} + c(\Delta t_a - \Delta t^{(i)}) + \eta_a^i + \epsilon_a^i \quad (2.29)$$

$$y_b^i = \rho_b^{(i)} + c(\Delta t_b - \Delta t^{(i)}) + \eta_b^i + \epsilon_b^i \quad (2.30)$$

where $\rho_a^{(i)}$ indicates the distance between a satellite i and receiver a .

2.7.2 Single difference estimator

In single difference estimators, illustrated in figure 2.2, the difference between two receivers is calculated, based on their relative distance to a satellite i , shown below when subtracting equation (2.30) from (2.29):

$$\begin{aligned} \Delta y_{ab}^i &= y_a^i - y_b^i \\ &= \rho_a^{(i)} + c(\Delta t_a - \Delta t^{(i)}) + \eta_a^i + \epsilon_a^i \\ &\quad - \rho_b^{(i)} + c(\Delta t_b - \Delta t^{(i)}) + \eta_b^i + \epsilon_b^i \\ &= (\rho_a^{(i)} - \rho_b^{(i)}) + c(\Delta t_a - \Delta t_b) - (\eta_a^i - \eta_b^i) + (\epsilon_a^i - \epsilon_b^i) \\ &= \Delta \rho_{ab}^{(i)} + c \Delta t_{ab} + \Delta \eta_{ab}^i + \Delta \epsilon_{ab}^i \end{aligned}$$

As presented in [18], with the same notation of Δ signifying a difference, this eliminates the satellite clock bias and orbit error, as well as atmospheric

interference being effectively removed for receiver separations less than 30 km. Receiver clock bias should still be estimated.

2.7.3 Double difference estimator

In order to remove the receiver clock bias, double difference can be implemented, illustrated in figure 2.3. This relies on the difference between two satellites, i and j , common between the two receivers. Introducing the symbol ∇ to signify double difference, the equations is set up as

$$\begin{aligned}\nabla \Delta y_{ab}^{ij} &= \Delta y_{ab}^{(i)} - \Delta y_{ab}^{(j)} \\ &= \Delta \rho_{ab}^{(i)} + c\Delta t_{ab} + \Delta \epsilon_{ab}^{(i)} - \Delta \rho_{ab}^{(j)} - c\Delta t_{ab} - \Delta \epsilon_{ab}^{(j)} \\ &= \Delta \rho_{ab}^{(ij)} + \Delta \epsilon_{ab}^{(ij)}.\end{aligned}\tag{2.31}$$

In equation (2.31) the receiver clock bias is eliminated. The atmospheric noise has been omitted as explained in section 2.7.2. Further, the relation between the relative position of two receivers is the dot product along a unit vector $\mathbf{e}^i = [e_x, e_y, e_z]$ pointing to a satellite i :

$$\Delta y_{ab}^{(i)} = \mathbf{e}^i \cdot \mathbf{r}_{ab}$$

and similarly, with a reference satellite j , the double difference distance is given by

$$\nabla \Delta y_{ab}^{(ij)} = (\mathbf{e}^i - \mathbf{e}^j) \cdot \mathbf{r}_{ab} + \Delta \epsilon_{ab}^{(ij)}.$$

Thus, given a set of $n + 1$ unit vectors pointing towards as many satellites, and their corresponding pseudorange measurements, a solution can be found utilising equation (2.25). Using satellite j as reference, with its corresponding direction unit vector and observation as reference gives the following vectors

$$H = \begin{bmatrix} \mathbf{e}^1 - \mathbf{e}^j \\ \vdots \\ \mathbf{e}^n - \mathbf{e}^j \end{bmatrix}, \quad \nabla \Delta \mathbf{y}_{ab}^{(j)} = \begin{bmatrix} \Delta y_{ab}^{1j} \\ \vdots \\ \Delta y_{ab}^{nj} \end{bmatrix}.\tag{2.32}$$

Equation 2.32 may be solved using the same least square method of 2.25 as the global position, but with the updated direction matrix.

Weighted least squares In [6] it is also suggested to use a BLUE estimator with the CNR in dBHz, denoted ψ , as an estimate of the noise level. The

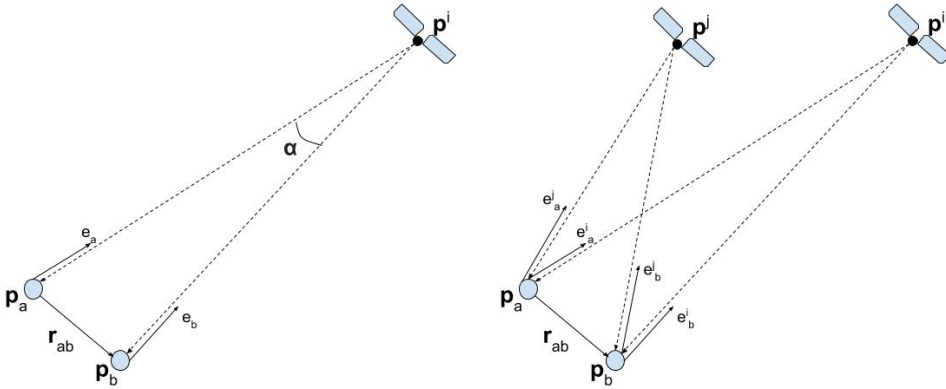


Figure 2.2: Single difference technique is able to estimate a relative position as well as eliminating satellite clock bias.

Figure 2.3: Satellite double difference can be calculated using two different satellites shared between the receivers

CNR value is registered by the receivers individually and is assumed inversely proportional to the variance of the noise of the observation σ^2 . The assumed variance of the noise for an observation between satellite i and receivers a and b is thus given by

$$\begin{aligned} (\sigma^{(i)})^2 &= (\sigma_a^{(i)})^2 + (\sigma_b^{(i)})^2 \\ &\propto (\psi_a^{(i)})^{-2} + (\psi_b^{(i)})^{-2}. \end{aligned}$$

The weight matrix W is proposed as a diagonal weight matrix expressed as

$$W = \text{diag} \left(\frac{(\psi_a^1)^2 \cdot (\psi_b^1)^2}{(\psi_a^1)^2 + (\psi_b^1)^2}, \dots, \frac{(\psi_b^n)^2 \cdot \psi_b^n}{(\psi_a^n)^2 + (\psi_b^n)^2} \right) \quad (2.33)$$

and the optimal solution is calculated as

$$\hat{\theta}_{BLUE} = ((H^{(j)})^T W H^{(j)})^{-1} (H^{(j)})^T W \nabla \Delta y_{ab}^{(j)}$$

as proposed in equation (2.28), and $(H^{(j)})$ and $\nabla \Delta y_{ab}^{(j)}$ are those presented in equation (2.32). Reference satellite j is chosen to be the signal with the highest CNR value for each epoch. For these cases notable increase in accuracy is shown, both compared to that of two global position estimates as well as an unweighted DD estimator.

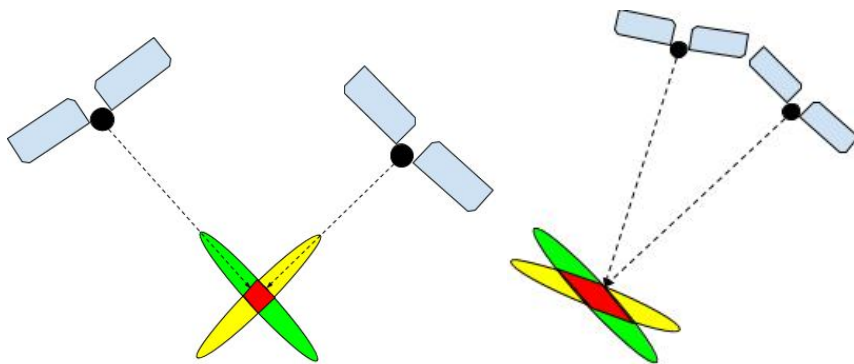


Figure 2.4: Illustration of the accuracy based on satellite constellation. Areas of high probability perpendicular to each satellite intersect, with the high probability intersection area marked in red. In the left image the angles between the satellites is large creating a small region, while in the right image the small angle yields a larger area.

2.8 Satellite Geometry

One important aspect of the accuracy is in the spread of the satellites the receiver can obtain data from. If all observable transmitting satellites appear in a high angle over the horizon - as can be the case in an urban environment with many tall buildings - the accuracy can be expected to decrease compared to a case with more spread out satellite constellation. As all observations measure a distance in one direction, if all observable satellites are positioned close to being in the same direction, then distance estimates in other directions become poor. This is illustrated for an artificial 2D case in figure 2.4 and is an effect of that close-lying points on a plane perpendicular to the radius all are approximately at the same distance from the center.

In relation to this, the dilution of precision (DOP) can be defined. This is a matrix quantifying the geometric distribution of the satellites in use. Defining the matrix $Q = (H^T H)^{-1}$, where H is the Jacobian of the geometric matrix in (2.20), gives an estimate of the uncertainty of the solution per direction based on the geometry of the observed satellites. q_{ij} is used to describe element row

and column, the following definitions are commonly observed:

$$HDOP = q_H = \sqrt{q_{11}^2 + q_{22}^2} \quad (2.34)$$

$$VDOP = q_V = q_{33} \quad (2.35)$$

$$PDOP = q_P = \sqrt{q_{11}^2 + q_{22}^2 + q_{33}^2} \quad (2.36)$$

$$TDOP = q_T = q_{44} \quad (2.37)$$

$$GDOP = q_G = \sqrt{q_{11}^2 + q_{22}^2 + q_{33}^2 + q_{44}^2} \quad (2.38)$$

Assuming that the geometric matrix is given in local NED coordinates, the HDOP, VDOP and PDOP respectively correspond to the horizontal, vertical and position uncertainty. TDOP is an estimate of the uncertainty in Δt_{rec} and GDOP the geometric uncertainty. This relation gives an estimate of how noise in the observation maps to an error in the respective estimate purely based on the satellite geometry. For this, the noise ϵ of each individual satellite should be assumed of equal magnitude [19].

The relation between satellite geometry and actual position uncertainty is expressed as a product of the noise level times the corresponding DOP value

$$\sigma_X = \epsilon \cdot q_X, \quad (2.39)$$

from which it is clear that the DOP value acts only as a scalar. For example, given a VDOP value of 3 and a white noise ϵ in the observations with a standard deviation of 1 m, discussed in section 2.2, can be expected to result in a standard deviation of 3 m in the vertical position. The actual noise level in the observations, the sum of all error sources discussed in section 2.2, called the User Equivalent Range Error (UERE), is however usually not known to the receiver.

The theoretically greatest achievable vertical spread is found with satellites under the receiver. This will not be achievable unless receiver is at a very high altitude since satellites below the horizon can't be observed. In practice an elevation threshold of at least 10° should be implemented since observations from low satellites have a higher noise level [20]. All observations in this paper have implemented a threshold of 15° , due to the treeline of surrounding forest at the site of observation being estimated to be in average at that angle from the horizon.

This leads to that the horizontal spread is mostly much greater than the vertical and the HDOP-value can be expected to be smaller than the VDOP-value by a

factor up to ~ 2.5 [21]. A GDOP value of 1 is considered ideal and should be considered good up to about 6 [22].

Chapter 3

Method

3.1 Simulation of data

Simulations of data are performed in order to verify the theoretical behaviour of the models under the influence of different noise levels. The global position estimator is verified for the influence on the position and clock bias estimates where noise levels of growing magnitude is introduced. The relative position estimate is also simulated and compared between two global position and the DD estimator, which will be compared to the result of the observations.

3.1.1 Testing different error sources impact on global position

The global positioning estimator's behaviour is tested using simulated data to verify the theoretical behaviour of the estimator. The simulations are based on creating pseudorange measurements between a stationary point on earth and corrupting it with noise, where actual receiver positions are used, and satellites are positioned according to the orbits from the data contained in the ephemeris messages.

The simulations are performed and evaluated in two ways:

- The convergence of the receiver state estimates for an error of growing magnitude.
- The trend of error in final state estimates for a noise of increasing mag-

nitude.

The noise types introduced are as follows:

- Initial position estimate error
- Receiver clock bias
- Satellite position random noise
- Measurement white noise
- Initial position and clock bias

Simulations of the initial estimate is simulated by setting the initial estimate θ_0 to be the sum of the true state θ and a random noise ϵ_p . ϵ_p is a 3×1 vector of Gaussian white noise, multiplied by a factor of increasing magnitudeWhen simulating a receiver clock bias, one random value is added to all observation. Satellite position random noise is simulated by introducing errors in all the satellite positions.

For a simulation with initial estimate error, as well as a receiver clock bias, the position estimate is expected to converge to zero with numerical precision. A combination of receiver clock bias and initial position estimate is also expected to converge to zero. When a random noise is added to the satellite position or observations, the estimate error is expected to grow at the same rate as that of the noise. From the simulations, the impact of different noise sources on the estimate can be analysed and used to identify potential errors in the estimation method.

3.1.2 RMSE of relative position from global position and DD estimate

Since the DD-method has been shown to improve the relative estimate as mentioned in section 1.6, the hypothesis is that the DD-method is superior to that of two individual global fixes in mitigating the effect of a common noise. The behaviour is simulated using increasing levels of bias. This means that any two simulated observations between a satellite and the receivers will be of the form

$$y_a = \|\mathbf{p}^{(i)} - \mathbf{p}_a\| + c\Delta t_a + \eta^{(i)} + \epsilon_a \quad (3.1)$$

$$y_b = \|\mathbf{p}^{(i)} - \mathbf{p}_b\| + c\Delta t_b + \eta^{(i)} + \epsilon_b. \quad (3.2)$$

The notation is consistent with that in section 2.7.1. In the simulations, the shared non-white noise $\eta^{(i)}$ is randomly sampled and will be constant per satellite for the observation series. This is a simplification, as the common noise is assumed slow changing. The simulations are performed using increasing magnitudes for the bias level. The result is then presented as the root mean square error (RMSE) of the estimate, defined as

$$\begin{aligned} e_{RMS} &= \sqrt{\sum |\mathbf{d} - \hat{\mathbf{d}}|/n} \\ &= \sqrt{\frac{1}{n} \sum_{i=k}^n (\mathbf{d} - \hat{\mathbf{d}}[k]) \cdot (\mathbf{d} - \hat{\mathbf{d}}[k])^T} \end{aligned} \quad (3.3)$$

for a true baseline vector \mathbf{d} and the corresponding estimated distance $\hat{\mathbf{d}}[k]$ for an epoch k . Since the experiment is conducted using the north and east direction separation, the baseline vector will be set to respectively $[10, 0, 0]$ m and $[0, 10, 0]$ m.

3.2 GNSS positioning from observation data

3.2.1 Data extraction from sensor

The INS unit allows for data sampling and streaming in real-time as well as logging for post-processing through three different types of software. A GUI called EvalTool is available from the producer Inertial Sense¹ for logging data for most applications, both fused and unfused data from the GNSS-receiver and the IMU units. In addition to that, there is a command-line tool called CL Tool for logging of much the same functionality². However, for the sake of this project, unprocessed pseudorange observation data from the receivers were required to implement and compare the single and double-difference methods described in chapter 2.7. In order to extract those, data must be parsed directly from the Software Development Kit (SDK) projects available. A logger, producing comma-separated values (.csv)-type log files of the received packages is available at <https://github.com/Kallemange/>

¹<https://docs.inertialsense.com/user-manual/software/evaltool/>

²<https://docs.inertialsense.com/user-manual/software/cltool/>

Communications for post-processing. More information on the logger and data structures in use can be found in appendix A.2.

3.2.2 Experimental setup

In order to test the receiver's behavior over time, two receivers are placed stationary at a baseline of 10 m pointing first in N-direction as well as in E-direction, with measurements taken for approximately 30 minutes in Ugglevikskällan, a glade in the forest on coordinates: 59.353°N, 18.073°E, shown in figure 3.1. One receiver was placed close to the pin indicated in the figure, and the other positioned east and south of it. The directions were set using a

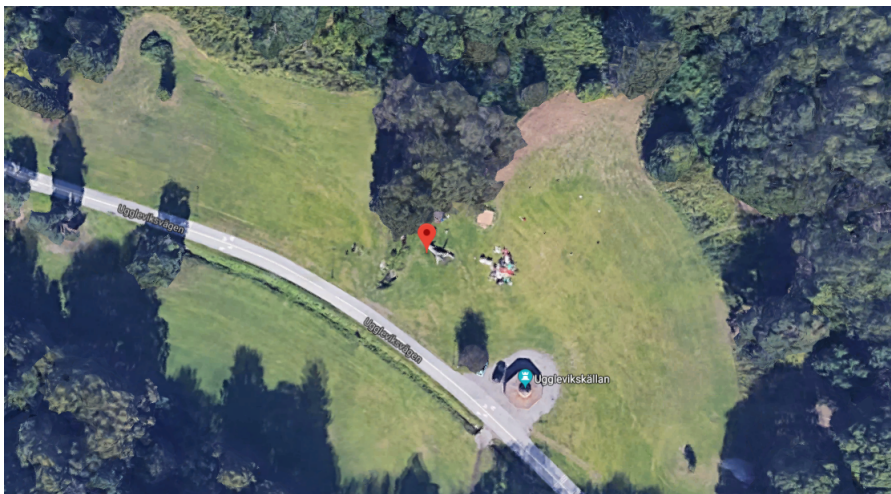


Figure 3.1: Uggleviken, place where observations were made. Image taken from Google Maps: <https://www.google.com/maps>

digital compass on an android phone and the distance through using a measuring tape. The logger is started for the receivers separately, but are connected to the same computer where the log files are stored.

3.2.3 Global and relative positions from onboard estimate

The onboard estimates are sampled and logged in parallel to the raw data. This contains information on the global position in an ECEF or LLA-frame, HDOP and VDOP values as well as sampling time. This data will be called

the onboard estimate. From this, an estimate of the variance in each direction can be made.

3.2.4 Global and relative position estimates from raw data

The method for how the positioning is made in the individual as well as the relative case using the log files is presented in the following section. The solutions have only been implemented based on log files and are not made to run real-time. The solution is calculated in two steps:

1. Load the data from log files into an array with a struct for each epoch.
2. Calculate the solution per epoch from the observation and ephemeris data

3.2.4.1 Global positioning

The positioning of each receiver only utilizes the ephemeris data collected by the same receiver and only observation data that has a corresponding ephemeris reading is used. The method for positioning which is implemented follows the description in section 2.5. The solution is an instantaneous estimate for each epoch, indicating that the previous estimate is not taken into account for the current one. This will produce a solution calculated in an ECEF coordinate frame, which is then projected to a NED frame. The solution includes a global position, calculated as described in section 2.5.1 with the weighted estimator of equation 2.27, an estimate of the HDOP and VDOP values, as described in (2.34-2.35) as well as a variance over the solution, calculated per direction in a NED-frame.

3.2.5 Double difference relative positioning

For the DD relative positioning algorithm, the set of satellites from which the receivers have sampled observations must be equal each epoch. Any observation not present in both is discarded. This method, which follows the algorithm for double difference in section 2.7 utilizes that the clock error cancels out and will not be estimated. The satellite position is instead calculated at the nominal time of observation t_{rec} . This is due to the angular change, as opposed

to the position change, between satellite and receiver is negligible within the time frame of a sample.

The relative position estimate also requires the receiver position \mathbf{p}_a , in order to calculate the unit vector \mathbf{e}^i pointing to a satellite from a receiver. The receiver position used is that given by the onboard estimate. The system of equations is then solved for the given reference satellite, which will be selected as that with the highest SNR value for each epoch, as suggested in [6]. The solution will give an instantaneous relative positional estimate for \mathbf{r}_b with regards to \mathbf{r}_a in an ECEF frame, which is then projected down to a NED solution through the point given. Given that the receivers were stationary, the estimates are expressed as a mean and a standard deviation in each direction.

Chapter 4

Results

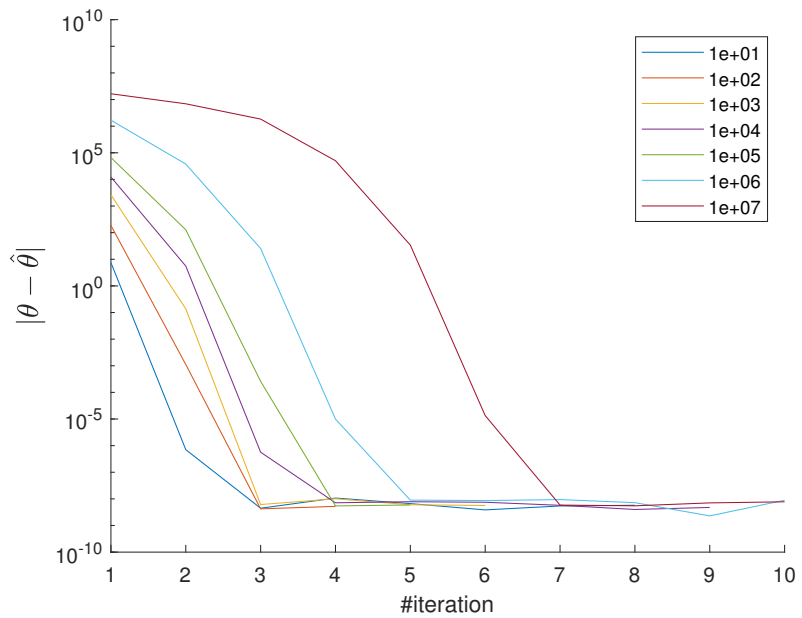
4.1 Error and convergence from simulated data

The results of the simulations on the influence of noise on the global estimator, explained in section 3.1 are presented in this section.

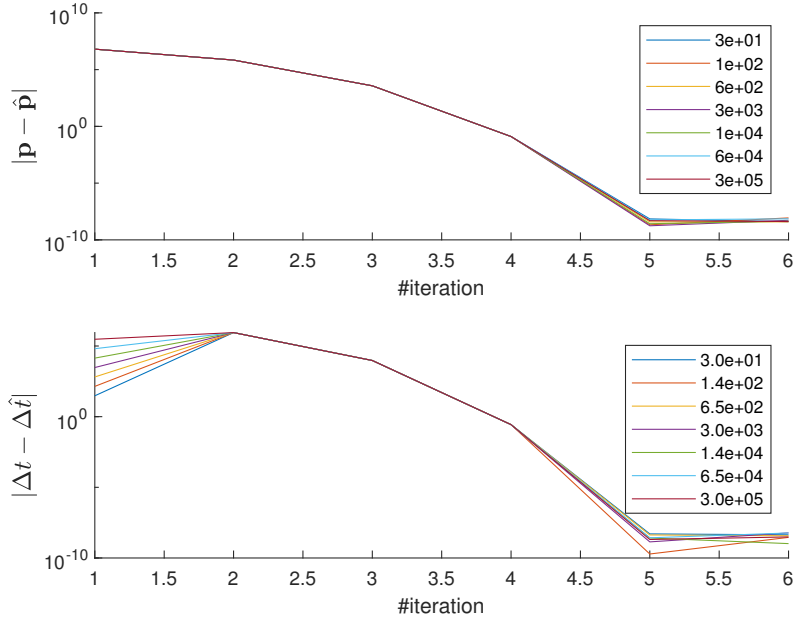
4.1.1 Convergence of estimate for noise free measurements with different initial error

The results of simulations of the convergence of the state estimates θ as a function of the number of iterations for is shown in figure 4.1. The simulations with initial estimate error were found to converge with an initial estimate error in the position of magnitude up to 10^7 m in all directions. The error in the final estimate is in the order of 10^{-7} . When adding noise to the satellite position or to the observations, a random noise is added to the satellite position of increasing magnitude from 1 to 10^4 m. These simulations indicate that the estimator behaves as expected since the final error grows equal to the noise.

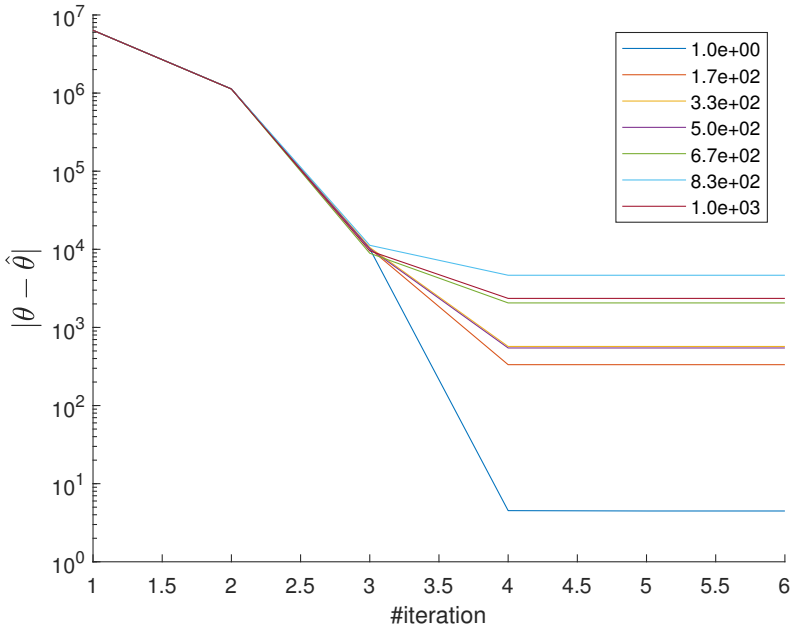
In figure 4.2 the convergence of an erroneous initial state with an added clock bias is presented. For any magnitude of initial error in all parameters between 10^{-10} to 10^4 m the parameters converge to the correct value within the interruption threshold of the estimator function.



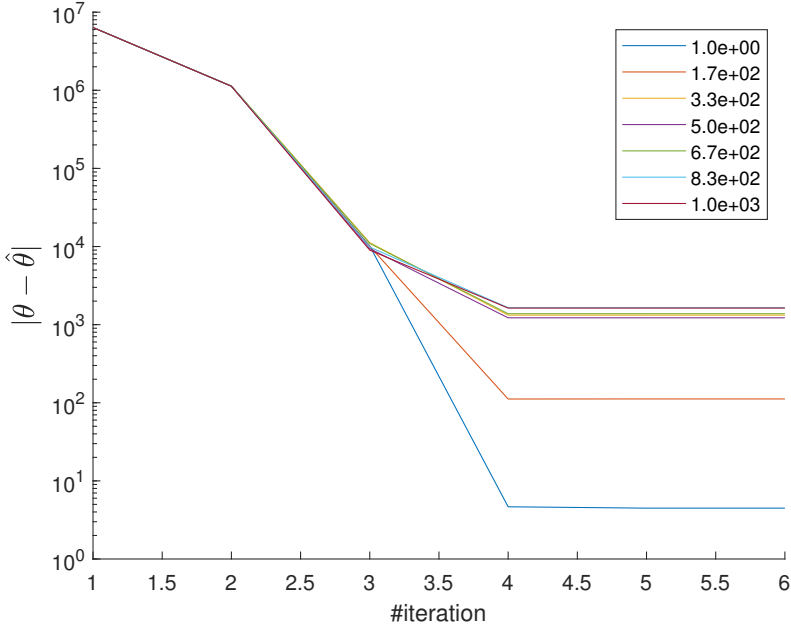
(a) Convergence of estimate error with a growing error in the initial position estimate.



(b) Convergence of estimate error with a growing receiver clock bias. Plot is split to show error in position (upper) and in clock bias (lower).



(c) Convergence of estimate error with a growing error in calculated satellite position.



(d) Convergence of estimate error with a growing added observation noise.

Figure 4.1: Simulation results with different input noise. The horizontal axis shows the number of iterations and vertical axis shows the norm of the error, where the estimate is indicated with a \wedge -symbol and the true value in the simulation without. Magnitude of the noise is indicated in the legend.

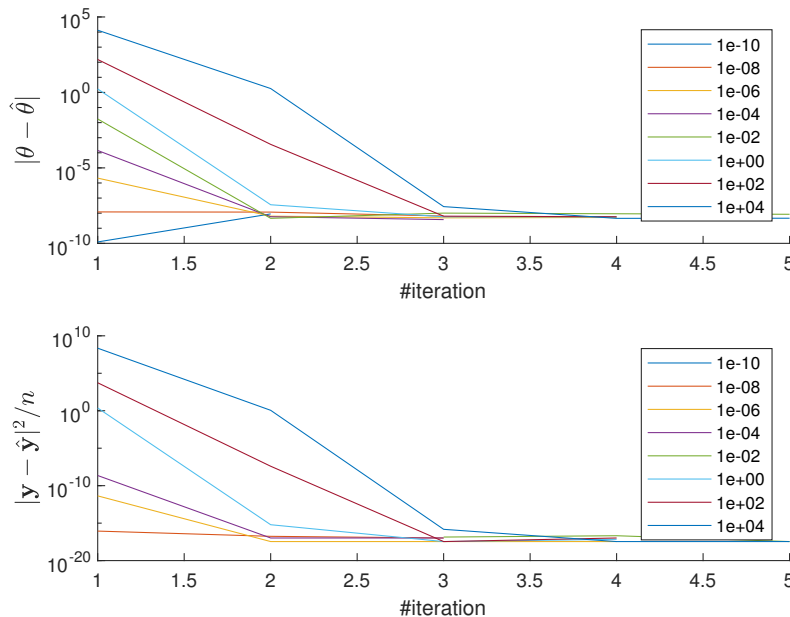
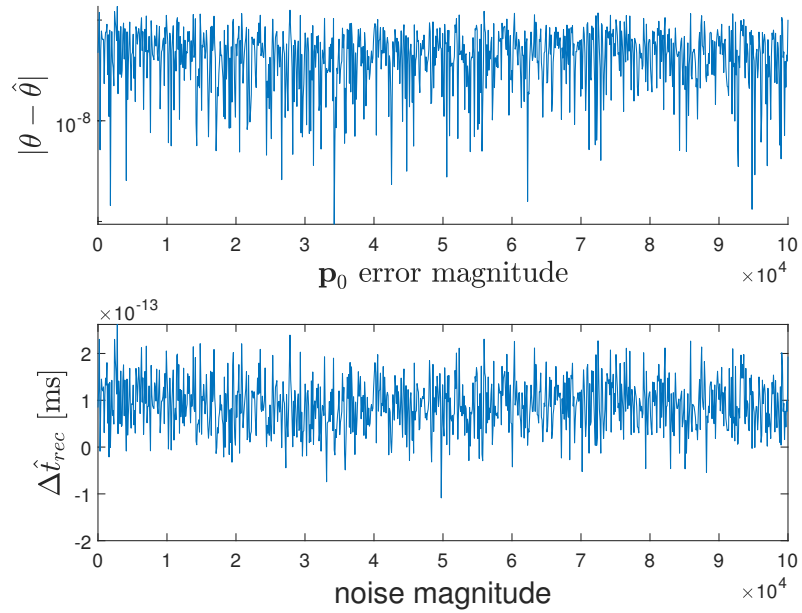


Figure 4.2: The plots show the convergence behaviour with noise free estimates and an initial random error in both position and clock bias of increasing magnitude. Upper: norm of error in state estimate per iteration. Lower: mean square error in estimated observations. \wedge -symbol indicates an estimate.

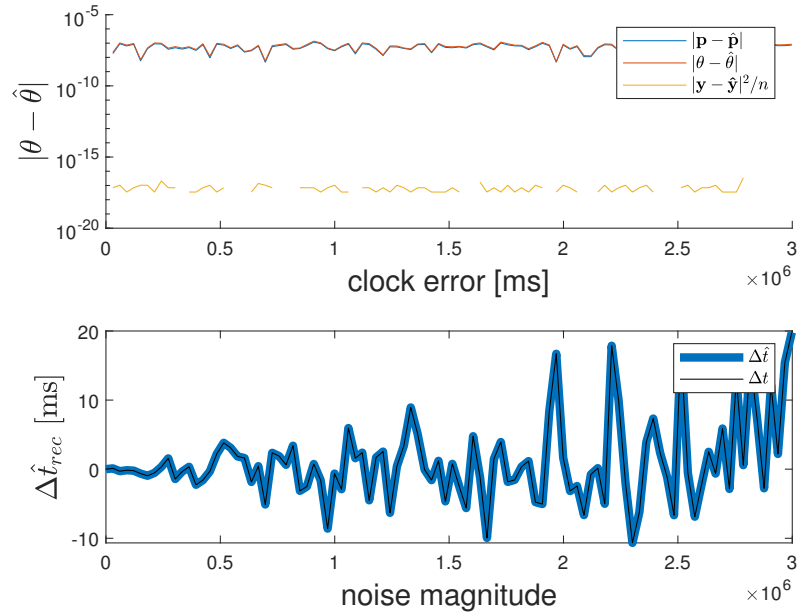
4.1.2 Final estimate for added measurement noise of different magnitudes

The simulated error in the terminal estimate of receiver states when adding noise of increasing magnitude is presented in figure 4.3. In the upper graph, three types of error in the estimates are shown: the norm of error in position, the norm of error in position and clock bias and the mean square error in the observations.

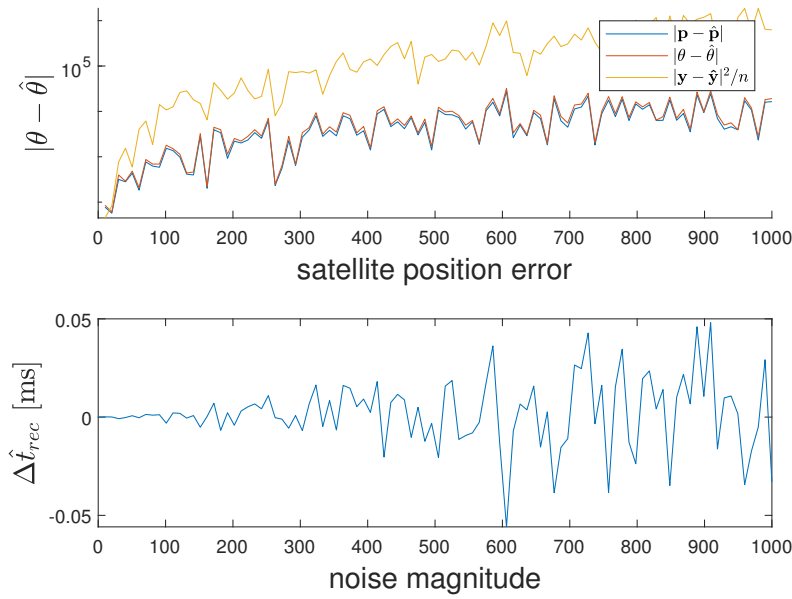
The simulations show that for an error consisting only of receiver clock bias, the effect on the positioning is negligible, as $|\mathbf{p} - \hat{\mathbf{p}}|$ lies steadily around 10^{-10} . For other types of added noise, the error appear to grow at the same rate as that of the noise source. This is an indication that the estimator functions as intended for simulated data.



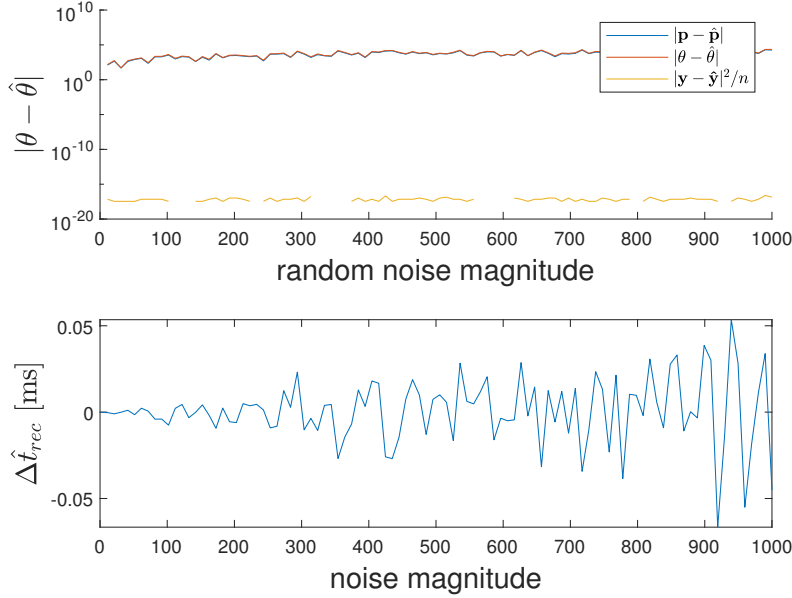
(a) Error in final estimate for an initial position error. Error in state estimate (upper) and estimated receiver clock bias (lower)



(b) Error in final estimate for a receiver clock bias. Error in state estimate (upper) and true and estimated receiver clock bias (lower).



(c) Error in final estimate with added satellite position error. Error in state estimate (upper) and estimated receiver clock bias (lower).



(d) Error in final estimate with added observation noise. Error in state estimate (upper) and estimated receiver clock bias (lower).

Figure 4.3: Simulation results with input noise of growing magnitude. Estimates are denoted with a \wedge -symbol, and true values without. The upper figure in each pair shows the norm of the error in position estimate, error in receiver state estimate and mean error in range estimate with a growing magnitude of the noise. In b), the true and estimated receiver clock bias are plotted together. Gaps in range error graph is due to round off error as value is close to zero.

4.1.3 Comparison of RMSE of relative position from simulated data

Simulations of the global position estimator and DD-estimator are done as described in section 3.1.2 using a Gaussian white noise level of 1 m. The positions are calculated first using two independent global fixes, and then the DD relative position with an increasing magnitude the common noise. In figures (4.4a-4.4c) the simulated results are shown of increasing the magnitude of the common noise which is set to respectively 1, 10 and 20 m.

It's apparent that for the global positioning the error grows with the common noise, while the DD-estimate position appears to be unaffected. This motivates the use of the DD-method for high levels of the common noise η shared between the receivers.

4.2 Individual and relative position estimate using global positioning

This section presents the results of the onboard estimate and the global position estimator, where positions are calculated individually. Sampling was performed for approximately 30 minutes per receiver in each direction. The results are presented in the form of:

- A histogram of the position estimate per direction per receiver.
- A plot of the position over time per direction.
- A table showing relative position and standard deviation.

4.2.1 Position from onboard estimate

The two individual onboard estimates is illustrated as a histogram in figures 4.5a-4.5b from a approximately 8500 samples per receiver. The estimate is transformed from an ECEF frame to a NED frame using the first registered position from receiver 1. Here the origin has been set to the mean over time for receiver 1 per direction. The ideal outcome would be positions separated by 10 m in one direction and 0 in the others and have a Gaussian distribution.

The standard deviation per direction and observation series is presented in table 4.1. σ_{12} has been introduced to denote the standard deviation in the relative estimate between the receivers. It is apparent from the images and the data in the table that the standard deviation of receiver 2 is greater than that of receiver 1 for all directions in both observations. It can be noted that receiver 2 is that which was placed close to the pin in figure 3.1 and was closer to the forest right north of it than receiver 1 for both observations.

	North	East	Down
E-dir			
Δp [m]	-11.5	-0.6	1
σ_1	0.8	0.5	1.7
σ_2	2.2	1.3	3.6
σ_{12}	2.4	1.3	3.9
N-dir			
Δp [m]	-2.4	10.9	-0.6
σ_1	0.9	0.6	1.5
σ_2	1	0.9	2.8
σ_{12}	1.3	1	3

Table 4.1: Mean and standard deviation of position from on board individual estimate, as well as the relative estimate. Values referring to the figures 4.5a-4.5b

4.2.2 Global and relative position estimates from global position estimator

The global position for two receivers is calculated as described in section 2.5 from received ephemeris and observation data. The observations are weighted using their respective SNR-value as described in equation (2.27). The results are based on approximately 8500 samples per receiver and observation series. They are presented in two ways:

- The positions are calculated independently for the receivers, using all available satellites.
- Only satellites which are shared between receivers are used.

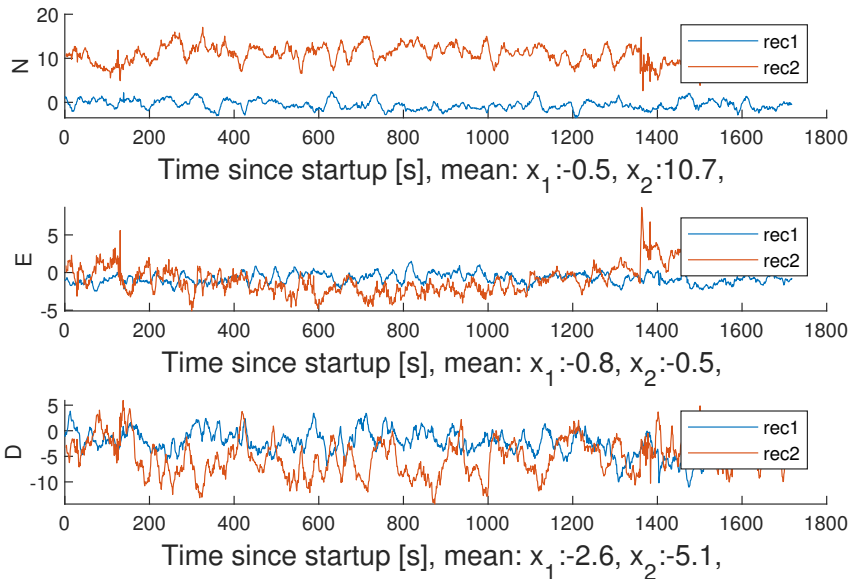
When fully independent estimates are used, several satellites may go in and out of tracking between two epochs, leading to a change in position estimate. The calculations when only shared information between receivers are used, only observations from satellites that were being tracked for the entirety of the observation series for both receivers were used and the rest discarded. The result of fully independent global estimates are presented in figures 4.6. The corresponding mean and standard deviation per direction for the two observations are presented in table 4.2a.

The results of independent global estimates where only shared information is used is presented in 4.7 and the corresponding mean and standard deviation per direction are presented in table 4.2b.

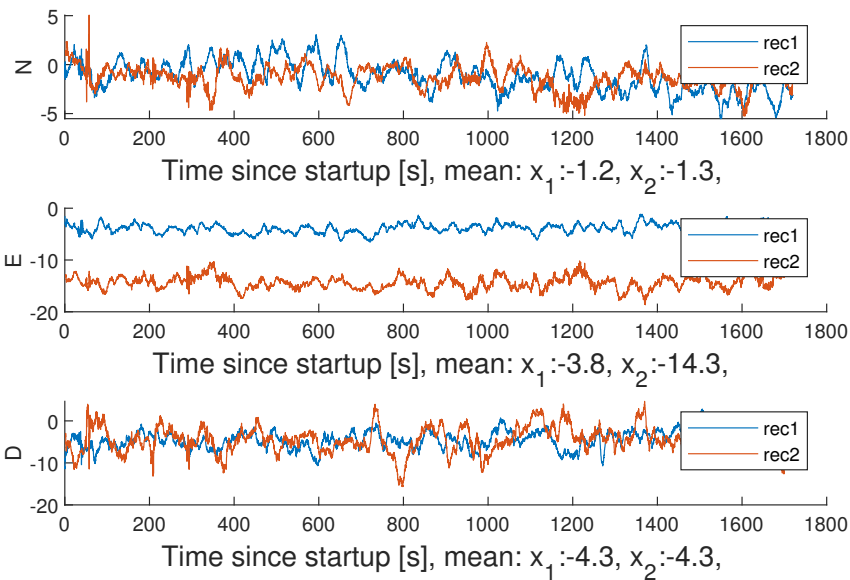
The results from table 4.2a and 4.2b are very similar, with a slightly higher error in position and standard deviation for the calculations where only shared information is used. As restricting the satellites to only using the shared information did not lead to improvements, no further results will be presented for this method.

A comparison between the onboard estimate and that of the global position estimator indicates that the onboard estimate is still superior. The estimate over time per direction for the two sample series, where they have been plotted together are shown in figure A.1. The position estimates from the onboard estimate and the global estimates from observation data are mostly very close and following the same trend, meaning that the estimates change similarly over time. It is however apparent that for some observations, the difference between the estimates becomes very large, in the order of several meters, as well as that the noise levels of the global position estimator are much larger than that of the onboard estimate.

The difference between the solutions are assumed stemming primarily from two sources: that the onboard estimate is filtered, as well as that it estimates the atmospheric noise. The filtering is indicated by that the position estimate follows a smooth curve without jumps between epochs. It is also likely that the ionospheric noise is estimated in the onboard position estimates. This has the potential to reduce the both the global and relative error significantly under the assumption that the noise is a common noise to both receivers, as shown in simulations in section 4.4.



(a) Position estimate in a NED-frame for separated by a 10 m baseline in a north direction.



(b) Position estimate in a NED-frame for separated by a 10 m baseline in an east direction.

Figure 4.6: Independent global position estimates for two receivers separated 10 m in N, E and D directions respectively. The origin is set to the first onboard estimate of receiver one. All satellite information known to respective receiver is used.

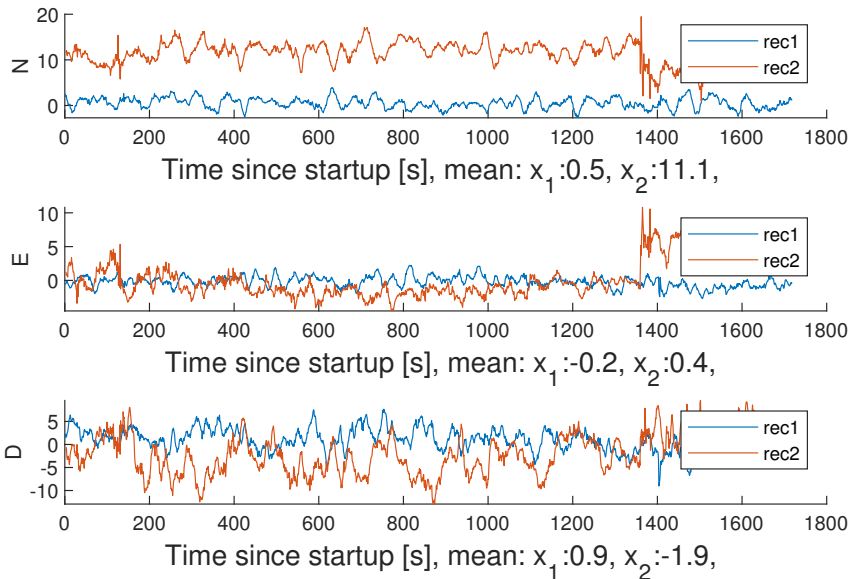
	North	East	Down
E-dir			
Δp [m]	10.2	0.3	-2.6
σ_1	1.6	0.9	2.2
σ_2	1.2	1.3	3.3
σ_{12}	2.3	1.8	4.2
N-dir			
Δp [m]	-0.1	-10.5	0
σ_1	1	0.7	2.4
σ_2	2	2.1	3.5
σ_{12}	2.5	3.3	5.5

(a) Values calculated for when receivers use all available information. Values referring to observation series shown in figure 4.6.

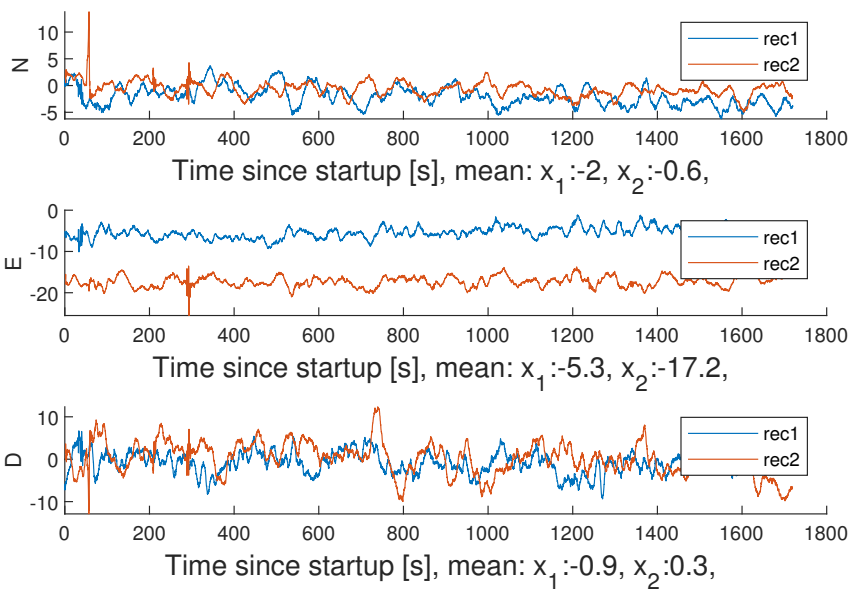
	North	East	Down
E-dir			
Δp [m]	10.6	0.6	-1
σ_1	1.8	1.4	2.5
σ_2	1.4	1.3	3.8
σ_{12}	2.2	1.9	4.3
N-dir			
Δp [m]	-1.4	-11.9	-0.4
σ_1	1	0.7	2.5
σ_2	2	2.1	3.5
σ_{12}	3.7	3.5	5.5

(b) Values calculated for when only satellites shared between receivers are used. Values referring to observation series shown in figure 4.7.

Table 4.2: Averaged values of difference in position, standard deviation of position estimate per direction and standard deviation of relative estimate.



(a) Position estimate in a NED-frame for separated by a 10 m baseline in a north direction.



(b) Position estimate in a NED-frame for separated by a 10 m baseline in an east direction.

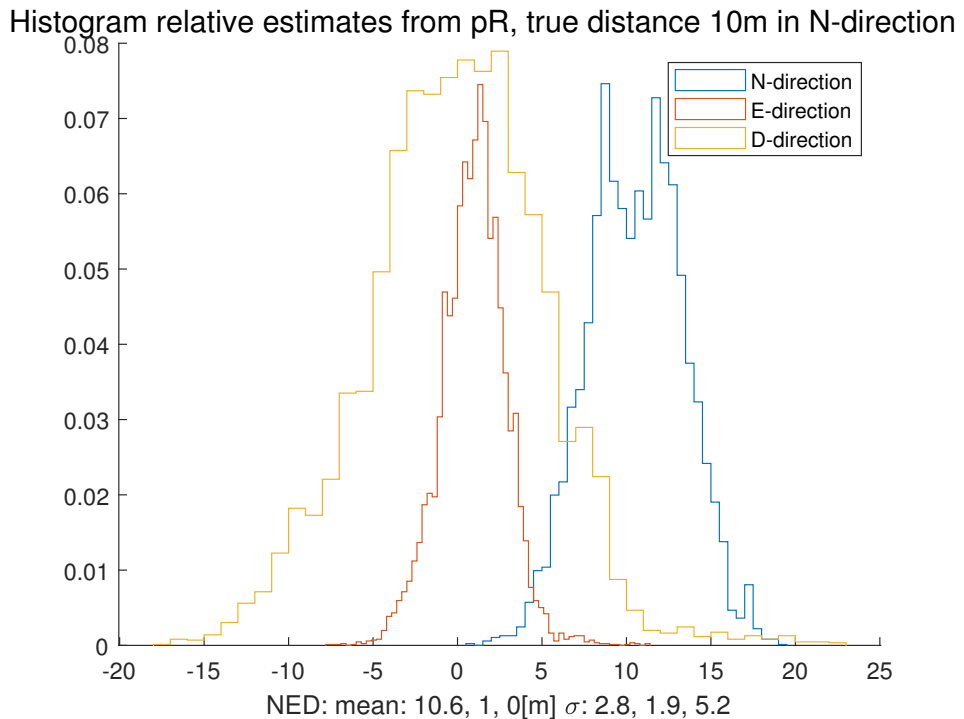
Figure 4.7: Independent global position estimates for two receivers separated 10m N-direction (upper) and E-direction (lower), origin is set to true position. Only satellite data shared between receivers is used.

4.3 Histograms of DD-relative position estimates

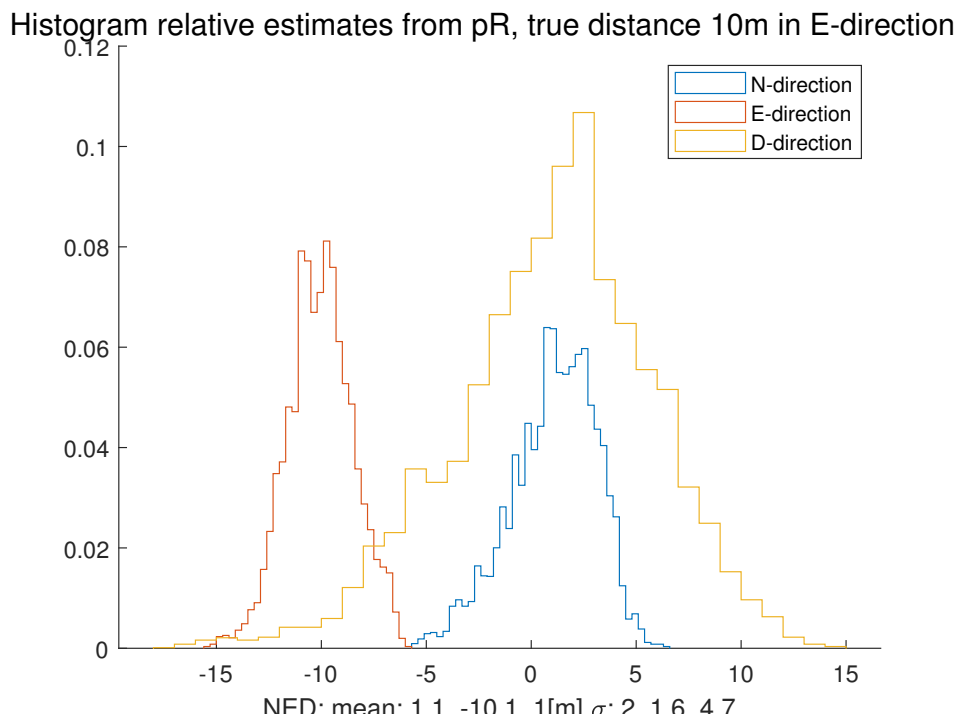
The DD-relative position estimates are calculated using the estimator described in section 2.7.3, using the observation weights in equation (2.33). Histograms of the relative estimates per direction are shown in figures (4.8a-4.8b). The mean and standard deviation for each direction of the two sample periods is presented in table 4.3. The estimates use the same data as those used in section 4.2.2.

The relative estimates from the global position and DD-estimator are similar and the DD-estimator shows a slightly higher standard deviation for the north-direction observation and slightly lower for the east-direction. Using these results there is no directly discernible difference in the performance of the methods.

The results from section 4.2.1 is also compared those presented in figures (4.8a-4.8b) in figures (A.2-A.3). The plots clearly show that the standard deviation of the DD-estimate at best is equal to, or close to equal to that of the onboard solution but generally can be expected to be greater.



(a)



(b)

Figure 4.8: Histogram over relative position estimate per direction from DD-estimator.

	North	East	Down
True[m]	10	0	0
Mean[m]	10.6	1.0	0.0
σ	2.8	1.9	5.2
True[m]	0	10	0
Mean[m]	1.1	-10.1	1.0
σ	2.0	1.6	4.7

Table 4.3: Averaged values of difference in position and standard deviation of position estimate per direction for a DD-estimate. Values referring to measurements in figure (4.8a-4.8b)

4.4 RMSE of relative position from observation data

The RMSE values of the relative estimates from observations, calculated in sections 4.2.2 and 4.3 are calculated. are shown in figures (4.9a-4.9b) with a 10 m separation in north and east direction separation respectively.

The calulaed RMSE values are, respectively for the global position and DD estimator 5.6 and 4.9 m in north direction, and 5 and 4.8 in east direction. The DD-estimator thus performs slightly better in both cases. This result is expected from the simulations in section 4.1.3, the decrease in error is however small. This indicates a higher level of random noise than expected in the observations.

4.5 DOP values

The DOP-values of the observation series are calculated as presented in section 2.8. The results from the global position and DD-estimator are presented in section 4.5.1 and 4.5.2 respectively. The DOP values are presented in order to find if any poor performance can be explained by the satellite geometry.

4.5.1 Global position estimator DOP values

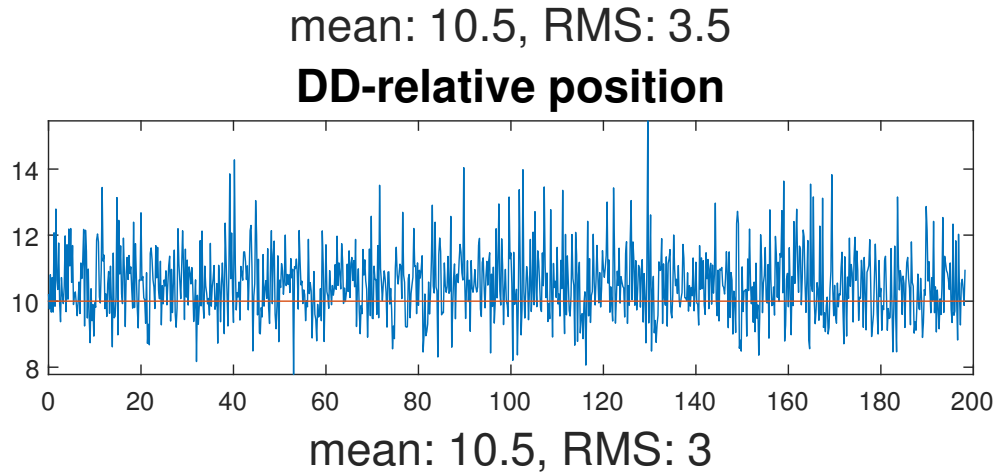
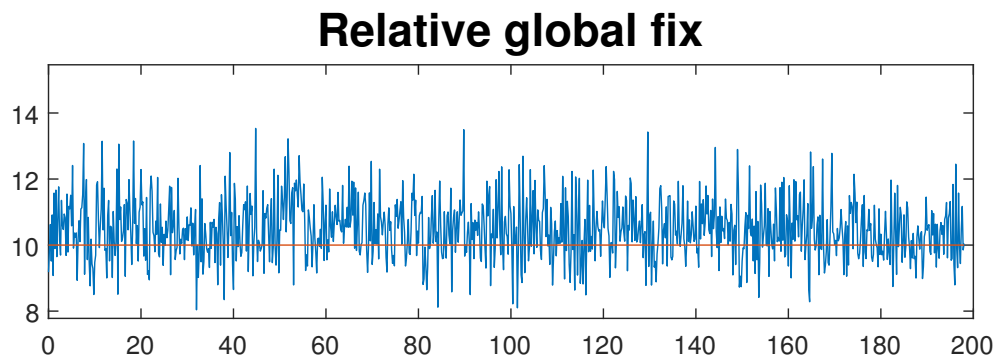
The DOP values from the observation series calculated for the global position estimator are presented in figure 4.10a-4.10b. The values are similar for receiver 1 and receiver 2 which is expected since only the difference in observed satellites should produce a difference in DOP-values with a short baseline distance. The HDOP and VDOP value with a mean of around 0.5 and 2 respectively at N-separation observation, and mean of around 0.45 and 1.6 for the E-separation observation. These are all well within the acceptable range of what can be considered good geometry, as presented in section 2.8 and it is unlikely that the high error in the relative estimates from the global position estimator presented in section 4.4 are due to the satellite geometry.

4.5.2 Double difference estimator DOP values

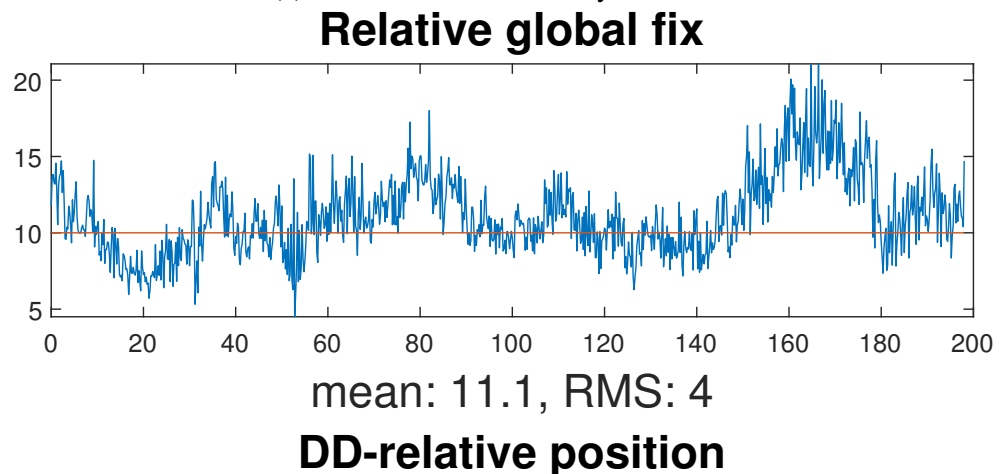
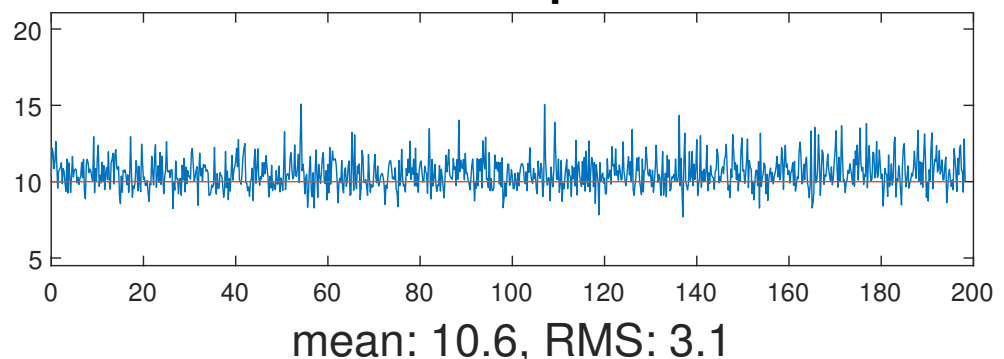
The DOP-values calculated for the DD-estimator differs from that of section 2.8 in that the TDOP-value is not included in the equations. This is due to that the receiver clock bias Δt_{rec} is not estimated. This results in the DOP-matrix being reduced to a 3×3 matrix. The GDOP value is thus calculated as

$$q_G = \sqrt{q_H^2 + q_V^2}$$

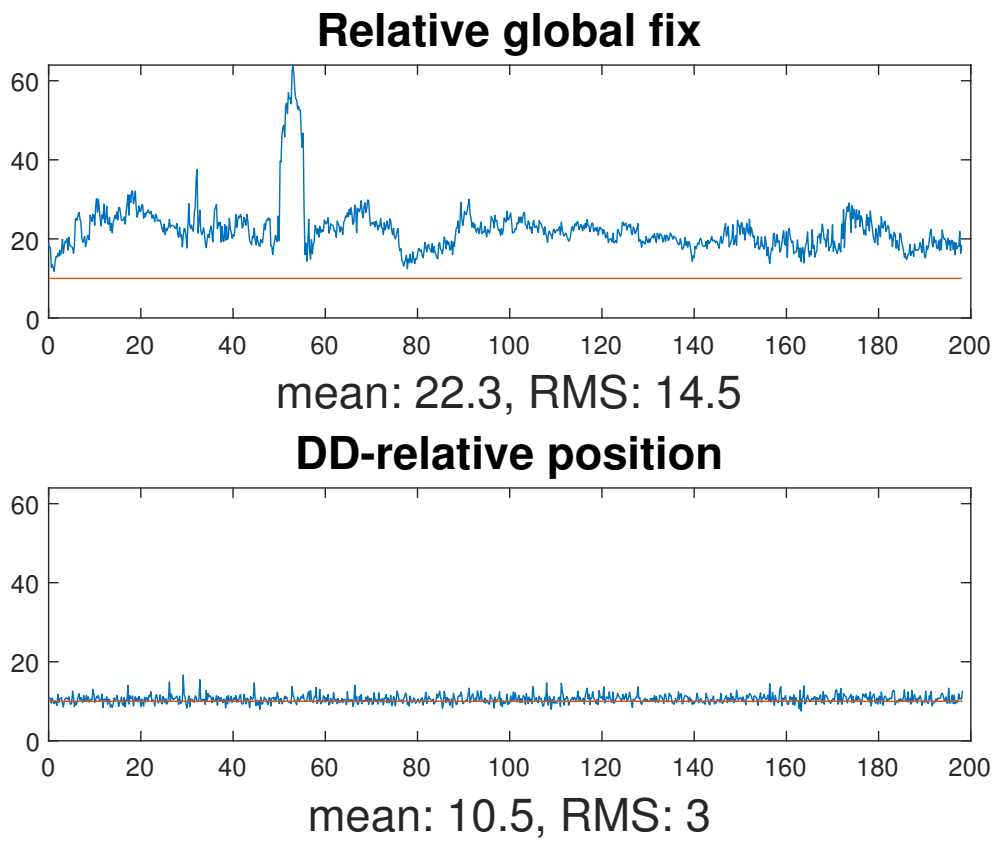
when the TDOP value is omitted. Besides that, calculations are performed equally. The calculated DOP-values are shown figures 4.11a-4.11b. The HDOP and VDOP values have a mean of 0.56 for the HDOP and 0.77 for VDOP in the N-direction separated observation, and 0.46 and 0.57 for the E-separated observation. This indicate that the satellite geometry was very good, with the exception of a few samples where it exceeds 3. Similarly to what was mentioned in section 4.5.1, the satellite geometry is unlikely to be a large factor in explaining the errors in section 4.4.



(a) Common noise scaled by a factor 1.

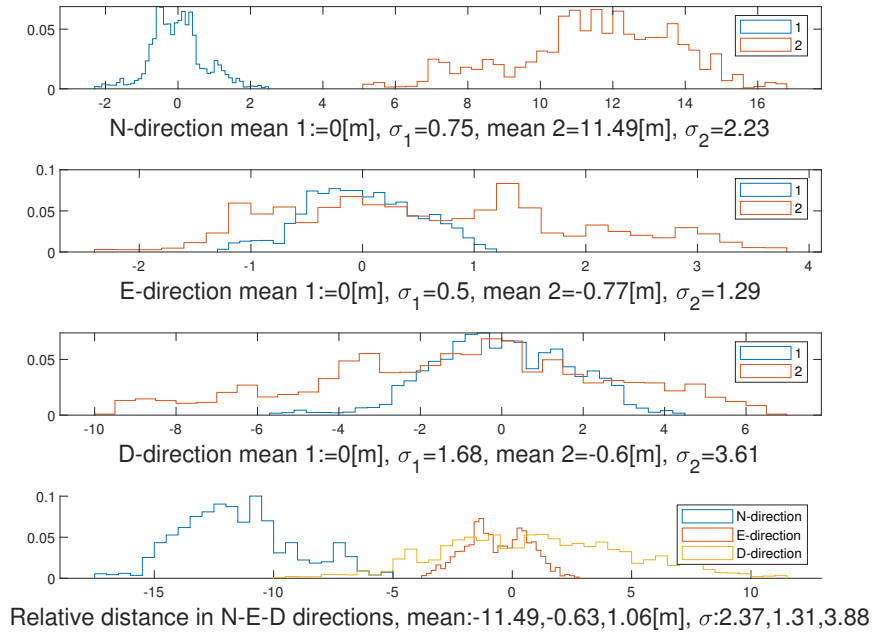
**DD-relative position**

(b) Common noise scaled by a factor 10.

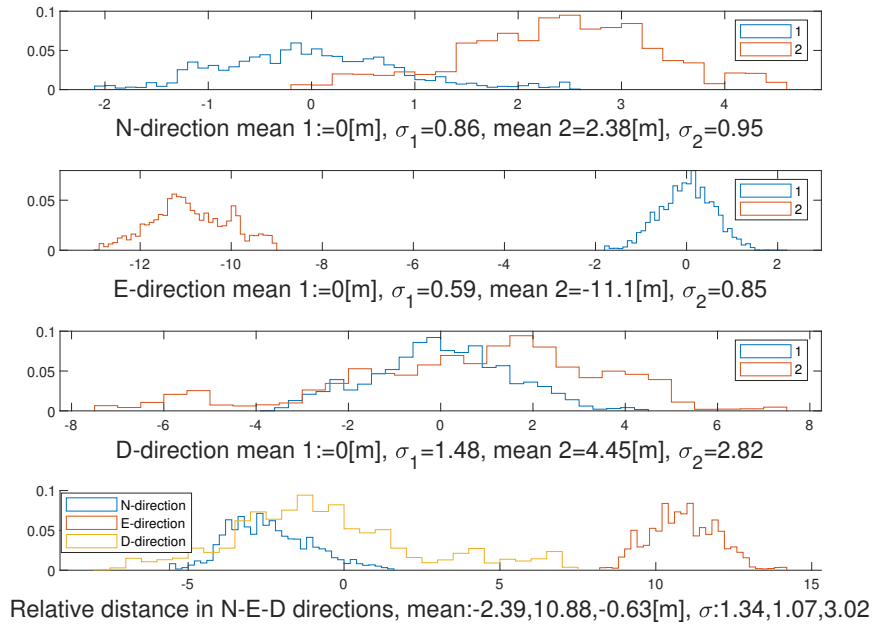


(c) Common noise scaled by a factor 20.

Figure 4.4: RMSE of global position and DD estimator from simulated data. The common noise $\eta^{(i)}$ for a satellite i is randomly sampled and scaled as indicated in the respective figure.

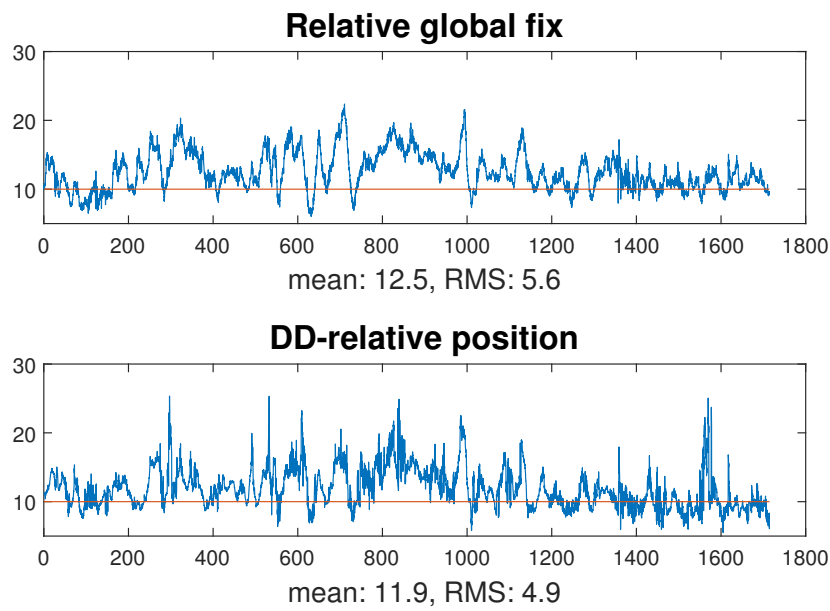


(a) Histogram over position estimate with an east direction separation.

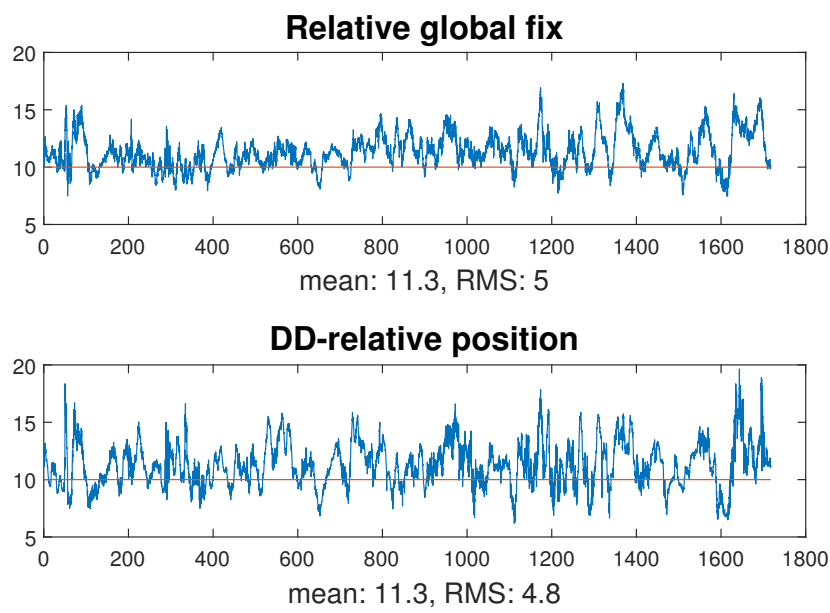


(b) Histogram over position estimate with a north direction separation.

Figure 4.5: Histogram showing position estimate over time with a baseline of 10 m separation between receivers from onboard estimate. For both figures: N-direction (upper), E-direction (second from top), D-direction (second from bottom), relative distance for all three directions at synchronised times (bottom). Origin is set to the first estimate of receiver 1.

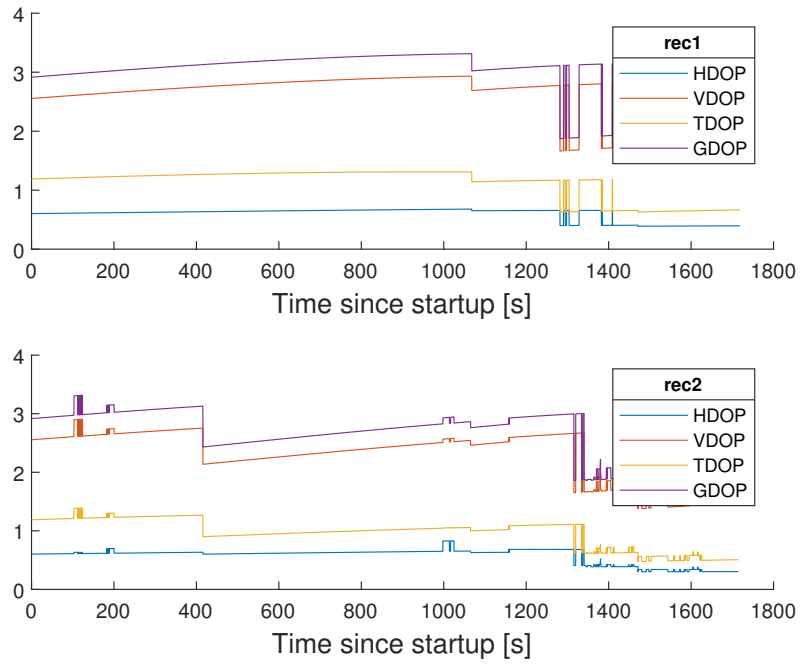


(a) Receivers separated 10 m in north direction.

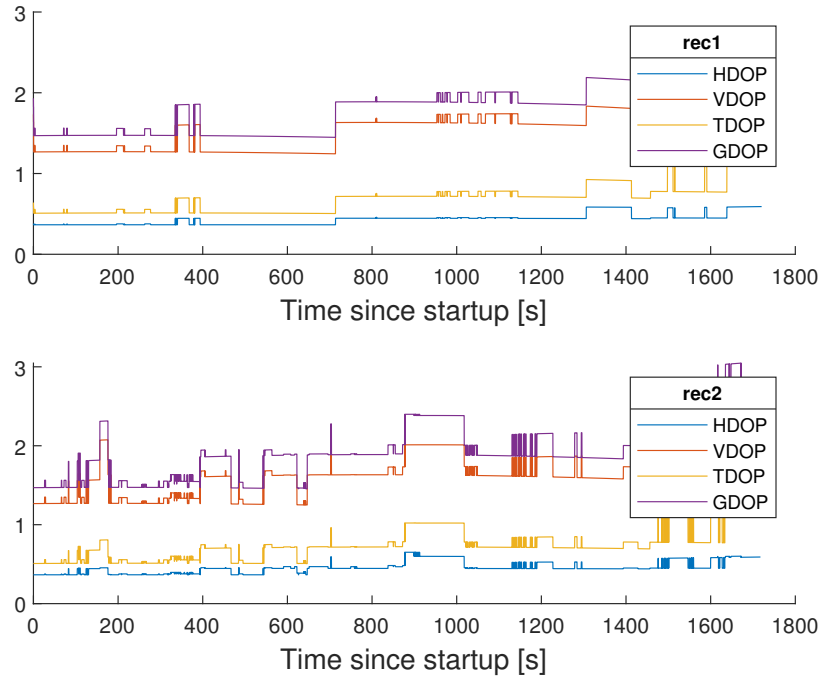


(b) Receivers separated 10 m in east direction.

Figure 4.9: Calculated RMSE of relative position from global position estimator and DD estimator from observation data. Receiver separation as indicated in the respective subcaption.

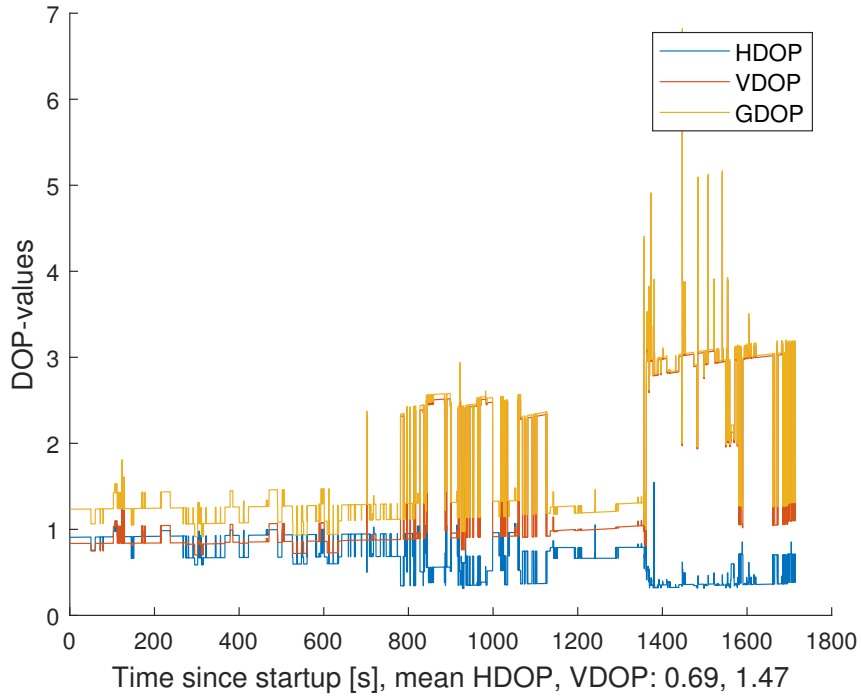


(a) Receivers separated 10 m in N-direction. Upper: receiver 1.
Lower: receiver 2.

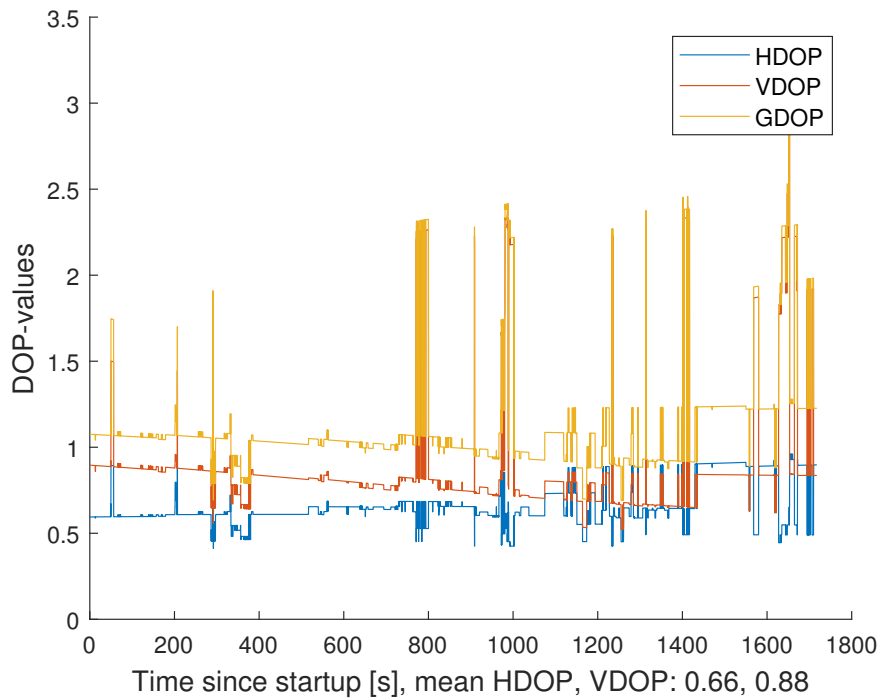


(b) Receivers separated 10 m in E-direction. Upper: receiver 1. Lower: receiver 2.

Figure 4.10: Individual DOP values for two receivers. Jumps in DOP-value between two epochs are due to change in which satellites are tracked by the receiver.



(a) Receivers separated 10m in N-direction.



(b) Receivers separated 10m in E-direction.

Figure 4.11: DOP values from DD-estimator. Jumps in DOP-values are due to changes in which satellites are tracked by the receivers, as well as a change in which satellite is used as reference.

Chapter 5

Conclusions and further work

5.1 Results of simulations

The results of the simulations presented in section 4.1 indicate that the implemented model works as expected as the error in position estimate grows equal to the noise in the input. It also verifies that the use of a DD-approach is meaningful when comparing the RMSE-values of an increasing signal bias, as illustrated in section 4.4. As the error of the DD-method is seemingly unchanged by the bias compared to the relative position of the global estimates, where it grows with increasing bias.

5.2 Precision of the estimates

The results that have been achieved point towards a slight improvement of an implementation of the DD-method, as compared to that of two individual position estimates. The large variance that was obtained in section 4.3 and 4.4 is however unsatisfactory with the ambition to reach below meter accuracy of the estimator. The answer to the question posed at the start of this project posed in section 1.8, seem to be that the noise level may very well be too large to reach the desired precision. The best results are still obtained from the solution directly sampled from the estimate of the onboard solution, as shown in figures (A.2-A.3). Part of the superior performance of the onboard estimate is presumably due to that its estimate is filtered, which can attenuate much of the high-frequency noise and perform outlier rejection. The big difference in

of the noise levels between the two receivers indicated both by the onboard estimate presented in section 4.2.1 as well as the implemented least squares estimate in 4.2.2 is assumed to be an effect of greater noise levels for the receiver placed closer to the forested area. If this assumption is true, the noise levels appear to vary much stronger based on the surroundings than was initially assumed at the beginning of this project.

5.3 DOP values

The results of the DOP-value calculations in section 4.5 indicate that a good geometry of satellites was available for all observations with the exception of a few observations. This comes as no surprise as the receivers had access to observations from more than 10 satellites from all epochs. The DOP-value is an important complement to keep track of in order to avoid situations of very poor geometry but may be of limited use to estimate actual errors as it doesn't contain information on the actual noise levels in observations.

5.4 Further work

Two suggestion for further work with regards to the high noise levels discussed in 5.2 are:

1. Implement a filtering process and outlier rejection for the raw observation data.
2. Verify this assumption of noise local noise differences by making observations at a more open place than that used for this project.

The method should also be implemented for real-time use, as the post-processing made only serves a theoretical purpose at the moment. Hopefully, the code which has produced these results can be used as a base for further development of a more useful implementation.

Appendix A

A.1 Least squares

Assuming that A is a matrix of size $m \times n$, where the rank is at least n , \mathbf{x} a vector of parameters and \mathbf{b} a vector of outputs, then the set of equations are expressed as

$$A\mathbf{x} = \mathbf{b}.$$

If $m > n$, the equation

$$A\mathbf{x} - \mathbf{b} = 0$$

generally doesn't have a solution. Instead, a cost function Q expresses the square error of the system, defined as

$$Q = (\mathbf{y} - A\mathbf{x})^T(\mathbf{y} - A\mathbf{x}) \quad (\text{A.1})$$

$$= \mathbf{y}^T\mathbf{y} - 2\mathbf{x}^TA^TA\mathbf{x} + \mathbf{x}^TA^TA\mathbf{x}. \quad (\text{A.2})$$

The vector $\hat{\mathbf{x}}$ is the parameters which minimizes the norm of Q , which is expressed as

$$\hat{\mathbf{x}} = \underset{\mathbf{x}}{\operatorname{argmin}}(||\mathbf{y} - A\mathbf{x}||). \quad (\text{A.3})$$

The solution to A.3 is found through finding the zeros to the derivative of Q with respect to all parameters in \mathbf{x} ,

$$\frac{\partial Q}{\partial \mathbf{x}} = -2A^T\mathbf{y} + 2A^TA\mathbf{x} = 0$$

which is where

$$A^T \mathbf{y} = A^T A \mathbf{x}. \quad (\text{A.4})$$

for some value $\hat{\mathbf{x}}$. Multiplying both sides with the inverse to $A^T A$ and thus the least square solution is given as

$$\hat{\mathbf{x}} = (A^T A)^{-1} A^T \mathbf{y} \quad (\text{A.5})$$

$$(\text{A.6})$$

A.1.1 Weighted Least Squares

This can be extended to a more general case to capture the uncertainties of the individual measurements. Assume that the matrix W contains the variances of the noise and is a diagonal matrix defined as

$$W = \begin{bmatrix} \sigma_1^2 & 0 & \dots \\ 0 & \sigma_2^2 & 0 \\ \vdots & \ddots & 0 \\ 0 & \dots & 0 & \sigma_m^2 \end{bmatrix}. \quad (\text{A.7})$$

Then a Best Linear Unbiased Estimator (BLUE) estimation can instead be given by:

$$\hat{\mathbf{x}}_{\text{BLUE}} = (A^T W A)^{-1} A^T W \mathbf{y} \quad (\text{A.8})$$

The full derivation of the BLUE model can be found in [23].

A.2 Data structs and log format

The INS unit provides several possible struct types of information which can be sampled at different frequencies depending on the type, where GNSS-signals can be sampled at up to 5 Hz, while the IMU offers sampling up to 250 Hz. Among them there are both relatively unprocessed as well as processed data. A few data structs have been sampled from in this project and will be described briefly:

- `ins_1_t` - Fused data from IMU and GNSS sensors, including position (LLA/NED), velocity (body frame) and sampling time.
- `gps_pos_t` - Pure GPS receiver processed data, including global position (ECEF/LLA), DOP, and sampling time.

- `gps_raw_t` - Raw observation data, including number of observations, data and data type (needed for the following fields).
- `obsd_t` - Raw observation data, contains receiver sampling time, satellite number, SNR (0.25dBHz), observation data carrier phase and observation pseudorange.
- `eph_t` - Satellite ephemeris data, contains information on satellite number, time of data transmission and time for ephemeris data issue, as well as all data mentioned in section 2.3.

The sampled data is saved in separate logs for each receiver for later processing. For the ephemeris log file the format is a single row for each observation including time of reception. For the observation data, the data in each epoch comes in a package of multiple observations. One whole package of observation will be logged in one row, with number of observation, time of reception shared for all followed by satellite data, SNR, loss of lock indicator, code indicator and observation data repeated in the following format:

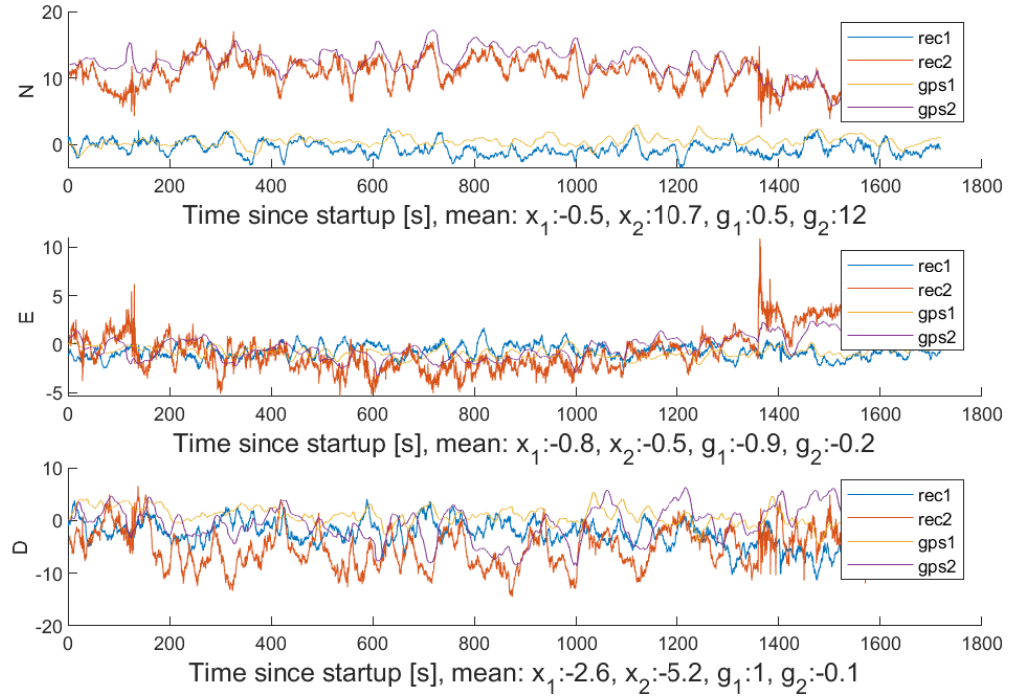
```
#obs, time1, time2, [satNo, SNR, LLI, code, P], [satNo, SNR, ...]
```

e.g.

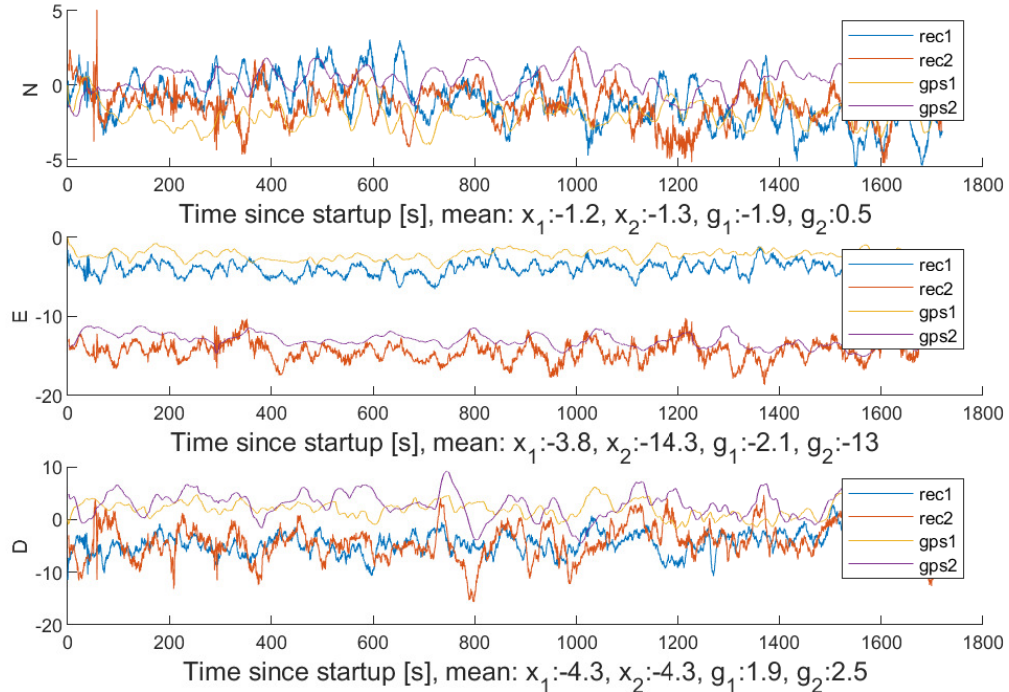
```
2,1562426103,0.391000,22,112,2,1,21772765.735608,41,76,0,1,20961030.484006,
```

A.3 Global position and onboard estimates

The position estimates from the onboard and global position estimator are shown together for the two sampling series in figure A.1.



(a) Position estimate in a NED-frame for separated by a 10 m baseline in a north direction.



(b) Position estimate in a NED-frame for separated by a 10 m baseline in an east direction.

Figure A.1: Independent global position estimates for two receivers separated 10m N-direction (upper) and E-direction (lower), origin is set to true position. The onboard estimate is plotted together with the global position estimator.

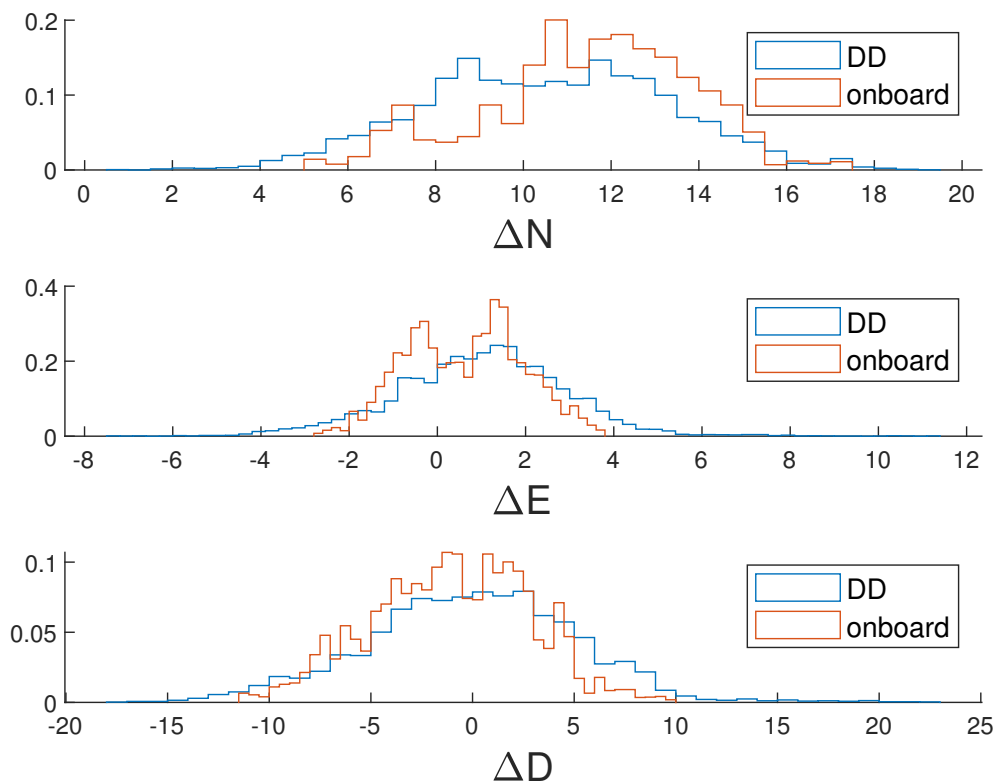


Figure A.2: Histogram over difference in position over time with a North direction baseline of 10 m. Plots showing results of DD and onboard solution.

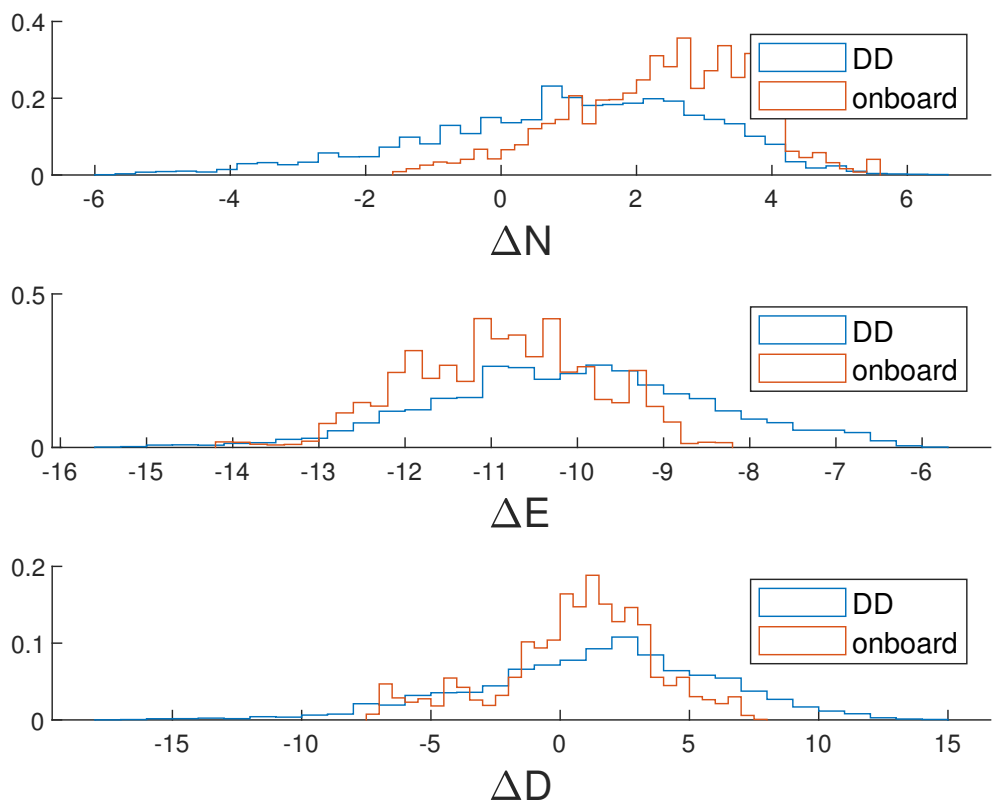


Figure A.3: Histogram over difference in position over time with an East direction baseline of 10 m. Plots showing results of DD and onboard solution.